Nonequilibrium Molecular Dynamics

William G. Hoover

Department of Applied Science
University of California at Davis–Livermore
Livermore, California

William T. Ashurst

Sandia Laboratories
Livermore, California

I. Introduction

Molecular dynamics is a product of today's fast computers. It is the solution of the classical equations of motion for up to several thousand simultaneously interacting particles. Such solutions, far beyond the reach of analytic methods, are crucial tests for approximate theories and often suggest how these theories can be made more nearly correct. Molecular dynamics has had a major impact upon statistical mechanics, the discipline that seeks to relate the gross macroscopic properties of molecular systems to those of the microscopic constituent molecules.

The constituent particles treated by molecular dynamics need not be simple point masses; polyatomic molecules, ions, or even stars can be treated. In any case the gross overall view of thermodynamics, hydrodynamics, plasma physics, or cosmology is replaced by a complete, detailed, particulate view—this detailed view is essential to any explanation of macroscopic behavior in terms of the properties of constituent particles.

Molecular dynamics can be applied to both equilibrium and nonequilibrium systems. How can we distinguish *non*equilibrium from equilibrium? According to thermodynamics, equilibrium is characterized by uniform chemical potentials, pressure, and temperature. All other properties of the system (specific heat, pair distribution functions, etc.) are then functions of the thermodynamic state specified by μ, P, and T. Nonequilibrium is characterized by *gradients* in the state variables or by values of these variables lying off the equilibrium μPT surface. Gradients lead to responding mass, momentum, and energy fluxes which eventually destroy the gradients unless these are maintained by external work. Thus *macro*scopic nonequilibrium systems are characterized by mixing and dissipation. On the *micro*scopic level of molecular dynamics the difference between equilibrium and nonequilibrium is less clear-cut. Indeed, the entire concept of microscopic equilibrium itself is elusive because chemical potential, pressure, and temperature have meaning only as averages, and all such averages fluctuate locally, even in isolated and undisturbed systems. A useful operational test for microscopic equilibrium is to see whether or not each average property of the investigated system lies within the range of equilibrium fluctuations. Thus, except near phase transitions, energy and momentum in a region with N particles should lie within ranges of order $N^{1/2}$ centered about the average energy and momentum. Any deviation much larger than this identifies a nonequilibrium system as such.

Nonequilibrium molecular dynamics often requires external force contributions in addition to the interparticle forces. These extra forces play the role of sources or sinks of work and heat and serve to link the N particles being studied to external boundaries or fields. The extra forces are required

because nonequilibrium systems imply dissipation, which is the conversion of work into heat.

Equilibrium systems are simpler. For a system of fixed composition, two independent "state variables" characterize equilibrium; average values in such a state are expected to be independent of the initial conditions for long enough computer runs. For a dynamic equilibrium system of fixed composition, the pressure and the kinetic energy (proportional to temperature) can be calculated and averaged as functions of volume and energy. For such equilibrium averages the dynamical method is unnecessarily complicated. The independent thermodynamic variables (N, V, and T, for instance) can be used to define an appropriate statistical partition function, and any of the dependent thermodynamic properties can then be determined from the partition function using the simpler Monte Carlo method (Ree, 1971; Wood, 1968).

Although characterizing a system as "equilibrium" or "nonequilibrium" presents a little difficulty, tracing the history of either sort of system is straightforward with molecular dynamics. The underlying principle is a simple one. We solve, with sufficient accuracy, the classical equations of motion

$$\mathbf{F}_i = m\ddot{\mathbf{r}}_i; \qquad i = 1, 2, \ldots, N, \tag{1}$$

if the system contains N structureless particles. If the particles are composite (polyatomic for example), then N would represent the total number of atoms comprising these particles. Each trajectory $\mathbf{r}_i(t)$ is then traced forward in time from the given initial conditions. In the equilibrium case, or the case of an isolated nonequilibrium system, all of the forces can be derived from a potential function $\mathbf{F}_i = -\nabla_i \Phi$, but that simplification is not essential.

Should the potential Φ be simple or complicated? Results and conclusions are most easily understood and generalized for simple potentials, such as the inverse powers; on the other hand it is certainly true that the ultimate theory has for its goal precise quantitative agreement with experiment. Potentials with as many as 11 constants have been used in order to describe real materials "realistically." Whenever calculations are primarily intended to aid the intuition, by suggesting or testing new approximations or correlations, Occam's razor should be used to simplify the forces.

Both the thermodynamic equilibrium view and the hydrodynamic nonequilibrium view reduce the number of degrees of freedom from those of the microscopic view. Molecular dynamics directly involves variables (the particle coordinates and momenta) hidden from macroscopic view. On a microscopic scale molecular dynamics is inherently a nonequilibrium method in which time and spatial averages always deviate somewhat from equilibrium values. Time averaging reduces the $6N$ variables of molecular dynamics to

the three thermodynamic state variables. The reduction in the number of variables achieved by hydrodynamics is more obscure. Hydrodynamic variables (number density, momentum density, and energy density, for instance) are defined at all points in space, implying at first glance an *infinite* number of degrees of freedom, not just $3N$. However, hydrodynamic quantities can be interpreted physically only in space–time intervals large enough to contain many particles. Otherwise fluctuations make the averages poor approximations. The number of hydrodynamic regions is ordinarily much smaller than the number of particles.

It is not easy to decide which variables and averages in a molecular dynamics problem are significant and worth saving, and which should be discarded. In nonequilibrium systems, just as in equilibrium ones, we want to concentrate our attention on properties that characterize well-defined nonequilibrium "states." Variables that fluctuate wildly or vary widely over a set of histories derived from similar sets of initial conditions are of less interest. (The N-particle distribution function is the extreme example of a function containing excessive information, exhibiting large fluctuations, and taking a long time—a Poincaré cycle—for its average value to converge.) Judicious choices of space and time meshes suitable for nonequilibrium problems have to be made. The space mesh has to be fine enough to describe significant gradients in composition, momentum, and energy; the time mesh has to be fine enough to describe significant relaxation processes. Because the relaxations are ordinarily achieved through dynamical particle interactions, the time mesh is ordinarily of order one collision time.

A. EARLY EFFORTS

Much of the pioneer molecular dynamics work was devoted to approaching and characterizing equilibrium. The characterization of equilibrium provided a check on the method because equilibrium results could be compared with those derived from the Monte Carlo method. Equilibrium systems were characterized by measuring long-time average values (for times long enough to dissipate the influence of the initial conditions) of pressure and temperature and functions of the fixed composition, volume, and energy.

The approach to equilibrium was examined in detail using molecular dynamics by observing the decay of some unlikely initial condition, such as all particles traveling with identical speeds or a single particle having initially all of the kinetic energy.

During the period from 1940 to 1970 the computer calculations established that (1) many systems *do* approach equilibrium in reasonably short times and (2) most thermodynamic properties of gases, liquids, and solids at equilibrium can be understood in terms of relatively simple theoretical

models. Perturbation treatments of the nearly ideal imperfect gas (Mayer and Mayer, 1940) and the nearly harmonic solid date back to the 1930s (Born and Huang, 1954). The semiquantitative theory of the liquid phase (Mansoori and Canfield, 1969; Rasaiah and Stell, 1970; Barker and Henderson, 1967; Henderson and Barker, 1970; Andersen *et al.*, 1971) developed much later. At present, interest has slackened in computer calculations of equilibrium properties for simple central force laws because the current nearly quantitative theoretical models make these largely unnecessary. Instead, most equilibrium calculations are exploring more specialized fields: mixtures (Rahman *et al.*, 1972), polyatomic molecules (Gibbons and Klein, 1974), quantum systems (Hansen and Weis, 1969), and relativistic systems (Guichelaar *et al.*, 1973).

How did the early molecular dynamic equilibrium calculations contribute to our understanding of the microscopic basis of thermodynamics? Simultaneous Monte Carlo statistical calculations showed that, within the numerical fluctuations common to computer calculations of practical length, the two computer methods were in agreement. This quantitative agreement between two independent calculations provided not only a welcome check of the numerical work but also an experimental proof that time and phase-space averages agree, within statistical fluctuations. This famous "quasi-ergodic hypothesis" can be used as a formal basis for statistical mechanics. It states that equilibrium properties can be obtained *either* by time averaging or by averaging with equal weights over all accessible states:

$$\langle f \rangle = \frac{\sum f_i}{\sum 1} \Leftarrow \frac{1}{\tau} \int_0^\tau f(t)\, dt, \qquad \text{for large enough } \tau. \tag{2}$$

Such a statement is fine for a relatively simple function f, such as pressure or potential energy, but *not* for very complicated functions. If, for example, one were to attempt the evaluation of the N-particle equilibrium spatial distribution function [known to be proportional to $\exp(-\Phi/kT)$ at temperature T, where Φ is the total potential energy function] through a time average, the time average would have to cover a period long relative to a Poincaré cycle time. A Poincaré cycle is the time required to traverse all states of interest at least once. These times are incredibly large, exceeding the age of the universe for N of order 10.

In the 1960s calculations showed that potentials incorporating a repulsion at short range and an attraction at longer range result in realistic phase diagrams with gas, liquid, and solid phases (Hansen and Verlet, 1969). See Fig. 1 for an example. The earlier hard-sphere work (Wood *et al.*, 1958; Wainwright and Alder, 1958) had shown that repulsive forces alone are sufficient to account for both the structure of the liquid phase and the melting transition linking the liquid and the solid phases. For two fluid
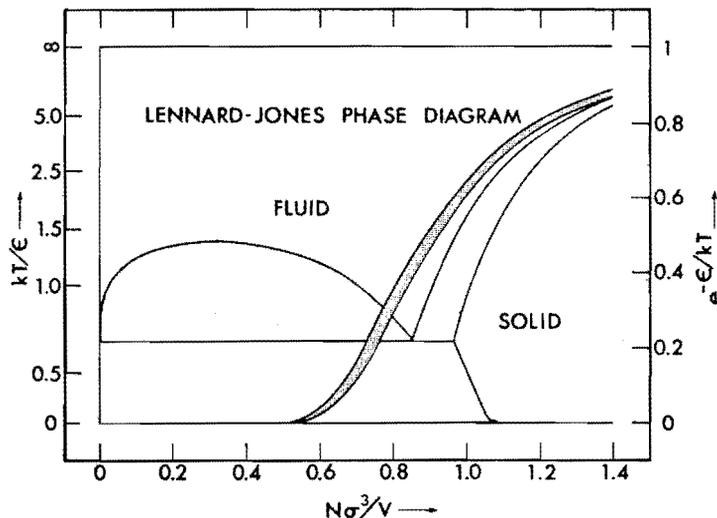
Fig. 1. Temperature-density phase diagram for particles interacting with the Lennard-Jones potential. Between the critical temperature, $kT/\varepsilon = 1.36$, and the triplepoint temperature, $kT/\varepsilon = 0.68$, two fluid phases, the gas and the liquid, can coexist. The phase diagram for the purely repulsive soft-sphere part of the Lennard-Jones potential $4\varepsilon(\sigma/r)^{12}$ is also shown. The shaded band of two-phase states separates the soft-sphere fluid phase from the face-centered-cubic solid phase.

phases to coexist, either attractive forces or very anisotropic forces (as in a liquid crystal) are necessary too.

B. Scope of Present-Day Work

What nonequilibrium problems should be solved, now that the approach to equilibrium and equilibrium itself have been characterized? The theoretical basis of nonequilibrium work is the Boltzmann equation (Chapman and Cowling, 1960); after decades in which experimentalists believed the equation to be established theoretically while theoreticians believed its foundation to be experimental (Barker *et al.*, 1971) a careful comparison of the two has established its validity at low density with small gradients. Within these density and gradient limitations, even *non*equilibrium systems are understood quantitatively. At higher density and with larger gradients the theoretical predictions are only semiquantitative and lie on empirical foundations. The traditional mission of the "kinetic" theory, the study of microscopic nonequilibrium systems, is threefold:

(i) to reveal the microscopic basis of the linear laws governing the diffusion of mass, momentum, and energy:

$$\mathbf{j} = -D\nabla\rho \quad \text{Fick's law for diffusion;} \tag{3}$$

$$\mathbf{P} = [P_0 - \lambda(\nabla \cdot \mathbf{v})]\mathbf{I} - \eta(\nabla\mathbf{v} + \nabla\mathbf{v}^\dagger) \quad \text{Newtonian viscosity;} \tag{4}$$

$$\mathbf{q} = -\kappa\nabla T \quad \text{Fourier's law for heat conduction} \tag{5}$$

(ii) to express the coefficient of diffusion D, the coefficients of viscosity λ and η, and the coefficient of thermal conductivity κ in terms of the microscopic force law; and

(iii) to determine the limits of (or corrections to) the linear relations linking the flux of particles $\mathbf{j}$, the flux of momentum $\mathbf{P}$, and the flux of energy $\mathbf{q}$ with the number density gradient $\nabla\rho$, the velocity divergence $\nabla \cdot \mathbf{v}$, the strain-rate tensor $\nabla\mathbf{v}$ and its transpose $\nabla\mathbf{v}^t$, and the temperature gradient ∇T.

Once these three tasks have been successfully carried out, macroscopic hydrodynamics, together with any extensions suggested by (iii) above, can then be used to solve particular problems of interest. This theoretical program has been successfully carried out *only* at low density (via the Boltzmann equation). So far, kinetic theory has failed to make quantitative predictions. This theoretical shortcoming leads to the present interest in the computer method of molecular dynamics.

In addition to these general kinetic-theory goals devoted to supplying the foundations for the macroscopic description of nonequilibrium systems, there are several additional areas in which the macroscopic approach is itself not particularly useful. In these areas the microscopic approach of molecular dynamics can contribute. If a system is either very small, or very far from equilibrium, the microscopic approach may well provide the *only* adequate understanding of "macroscopic" properties. Examples include strong shockwaves (Bird, 1970), plastic flow of solids, the damage caused in solids by radiation (Gibson *et al.*, 1960; Erginsoy *et al.*, 1964); surface structure (Lee *et al.*, 1974), and the propagation of cracks (Gehlen *et al.*, 1972). We will assess the progress and the prospects for both kinds of calculations, those which support hydrodynamics, and those which lie outside its scope.

II. Molecular Dynamics

A physical system to be studied by molecular dynamics involves interacting particles, boundaries which contain these particles, and external forces which interact with the particles. The simplest problem in molecular dynamics eliminates two of these three components and follows the motion of an isolated system of particles in a *periodic* box. A periodic box is one in which a particle "leaving" the system simultaneously reenters on the opposite side. The periodicity eliminates surface effects so that only particle–particle interactions need be included. If the interparticle forces are conservative, then mass, momentum, and energy are all constants of the motion. In the usual case the forces are taken to be sums of pair contributions:

$$\mathbf{F}_i = -\nabla_i \sum_{j \neq i} \phi(r_{ij}). \qquad (6)$$
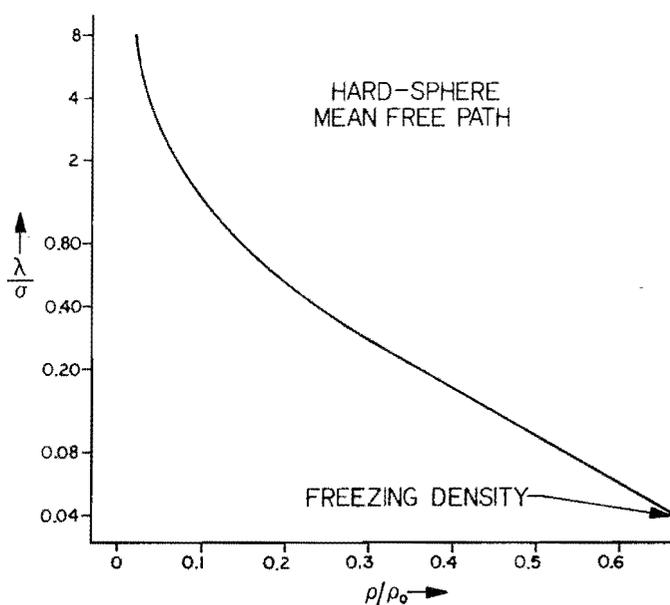
Fig. 2. The hard-sphere mean free path, for spheres of diameter σ, as a function of density. The close-packed density is ρ_0.

If the density is low enough (comparable to atmospheric density or less), then the dynamical problem can be simplified, treating the collisions statistically, from the low-density Boltzmann equation viewpoint. The Boltzmann equation is based on the assumption that particle collisions involve isolated pairs of uncorrelated particles. This assumption should hold when the time between collisions corresponds to a path much longer than the range of interparticle forces. Figure 2 shows how the mean free path for hard spheres depends upon density. In order for this path to reach 100 hard-sphere diameters the density has to be reduced to about one thousandth of the close-packed density. At high density particles become correlated with their neighbors; near the freezing point a particle spends most of its time in strong interaction with *several* neighbors, not just one. Thus a dense-fluid particle trajectory (Fig. 3) is more complicated than the series of straight line segments between infrequent collisions visualized by the Boltzmann equation. In dense fluids no quantitative statistical simplication is possible, and the equations of motion have to be solved exactly.

A. GENERATING TRAJECTORIES

At least five separate schemes for solving the equations of motion have been used (Gibson *et al.*, 1960; Rahman, 1964; Harp and Berne, 1968; Verlet, 1967; Aarseth, 1972). Because all of these schemes appear to produce
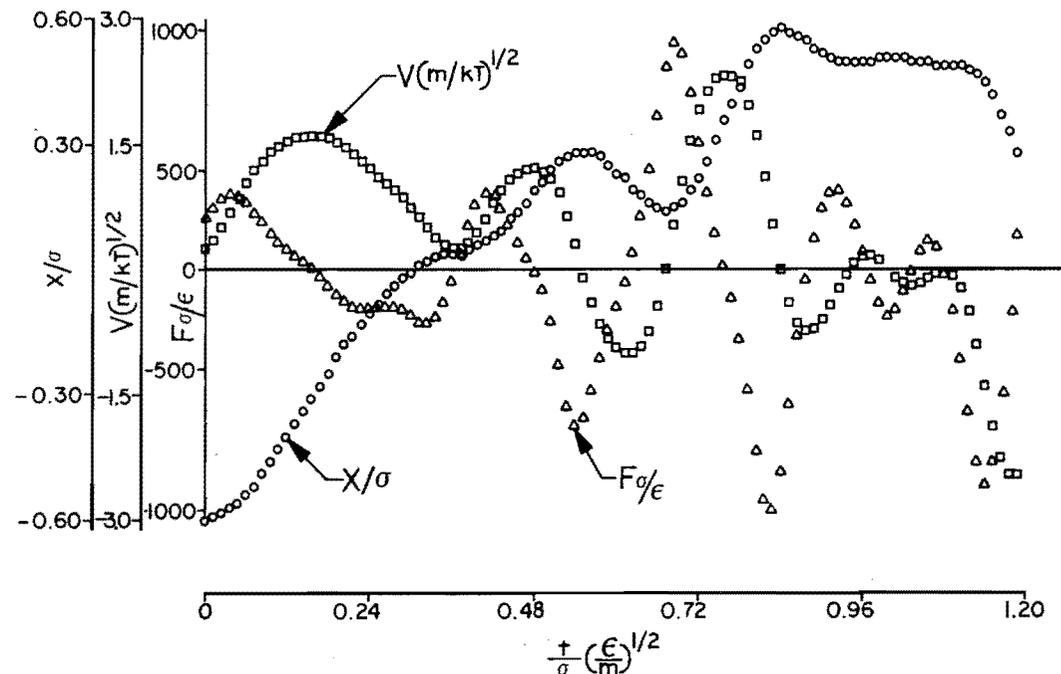
Fig. 3. Portion of a typical particle trajectory in a Lennard-Jones simulation of liquid argon at its triple point. The components x, $\dot{x}$, and $\ddot{x}$ are shown for a time interval of approximately 1 psec (10^{-12} sec). Individual values are shown for the 100 time steps of 10^{-14} sec each.

results of similar accuracy with similar investments of computer time, we describe only the simplest, Verlet's:

$$\mathbf{F}_i(t) = m_i[\mathbf{r}_i(t + dt) - 2\mathbf{r}_i(t) + \mathbf{r}_i(t - dt)]/(dt)^2. \tag{7}$$

If a record is kept of the coordinates at the current time t [from which $\mathbf{F}_i(t)$ can be calculated] and at the previous time $t - dt$, then *new* coordinates, at time $t + dt$, can be calculated by solving this equation for $\mathbf{r}_i(t + dt)$. The time interval has to be chosen *large* enough (otherwise the particle trajectories traced out in the available computer time will be too short) and also *small* enough (if dt is too large, then the difference equation fails to conserve energy and is a poor approximation to the differential equation of motion). In a dilute gas dt would have to be small enough so that the duration of a single collision (of order one picosecond at room temperature, 10^{-12} sec) spans several time steps. For a dense fluid, or solid, dt should be chosen so that a typical particle's vibrational period takes of order ten time steps (Fig. 3).

Notice that the velocities of the particles never explicitly enter Verlet's formulation of the equations of motion. These can be calculated, with errors of order $(dt)^4$, from the centered difference equations

$$\mathbf{v}_i(t) = [\mathbf{r}_i(t - 2\,dt) - 8\mathbf{r}_i(t - dt) + 8\mathbf{r}_i(t + dt) - \mathbf{r}_i(t + 2\,dt)]/(12\,dt). \tag{8}$$

If the force law has a complicated functional form such as the 11-constant one used by Lee *et al.* (1974) to represent argon, a time-saving alternative to the calculation of the interparticle forces becomes attractive: the forces can be tabulated as numerical functions of the interparticle separation. Six-figure accuracy can be obtained easily. The process just outlined, in which the forces are either calculated or tabulated, can be used to generate trajectories with up to several million time steps. The number of time steps is limited primarily by the cycle times of the fast computers used. At present these times are of order 10 nsec (10^{-8} sec). When the trajectories have been constructed the "molecular dynamics" problem has been solved. What then remains to be done is to interpret the data, deciding which variables or averages best represent the results.

B. REVERSIBILITY OF TRAJECTORIES

To be strictly correct we have to qualify the claim that we can "solve" the equations of motion. It is worth noticing that our solution of the *difference* equations of motion is qualitatively different from the true solution of the *differential* equations of motion. The reason is that *any* slight error in a particle trajectory (such as the apparently minor error induced by keeping only 14 significant figures!) grows exponentially large with time. Ultimately the particle's collision sequence differs qualitatively from that characterizing the true solution (with an infinite number of significant figures). This same exponential growth in the trajectory error is responsible for the surprisingly small number of times an elastic sphere can bounce on a similar sphere initially two diameters below it, taking into account the momentum uncertainty implied by the uncertainty principle of quantum mechanics. In *any* computer simulation the reversibility of the equations of motion is ultimately destroyed by the error produced in the last significant figure kept in the particle coordinates. This is true even with Verlet's scheme which is in principle reversible (symmetric in the time) if roundoff error is ignored. Despite the irreversible character of computer simulations there is no evidence that the "solutions" obtained differ in any thermodynamically or hydrodynamically important way from true solutions of Newton's differential equations of motion.

It is true in principle that more nearly accurate difference schemes, with error terms of higher order in dt, can be derived by combining coordinate values at ever greater numbers of discrete times. The actual gain in accuracy does not seem to justify the extra programming effort involved. From the physical point of view it is clear that eventually, usually in a few time steps (see Fig. 3), a particle has forgotten its past history. Information along its trajectory at even earlier times therefore is of little value and may even be misleading in trying to predict the future. Thus the smooth, analytic nature

of the trajectories should not be taken too seriously. Even for the relatively simple trajectory of an harmonic oscillator, with frequency ω, 27 terms in the expansion of $r(t + dt)$ would be needed to calculate $r(t + \omega^{-1})$ with six-figure accuracy. The most efficient use of computer time appears to lie with low-order difference schemes such as Verlet's coupled with a relatively small time step.

C. IMPULSIVE FORCES

The pioneering calculations of the 1950s (Alder and Wainwright, 1958, 1959) used impulsive forces (infinite, but acting over zero time to produce instantaneous momentum changes) derived from the hard-sphere and square-well potentials. In these cases the particles *do* travel along straight line segments between isolated binary collisions, even at high density. In order to avoid making trajectory errors of order dt, it is necessary to use a different dynamical method for hard spheres and square wells: the precise times associated with each collision are calculated accurately and the particles are advanced in time to their next collision; thus dt varies with time. Figure 4 illustrates the hard-sphere and square-well potentials along with the four kinds of collisions which are possible with the square-well interaction. These simple potentials played valuable roles in establishing the approach to equilibrium (Alder and Wainwright, 1958) and the number-dependence of thermodynamic properties (Hoover and Alder, 1967). Pair distribution and free-energy functions derived from the hard-sphere work made it possible to develop the successful perturbation treatment of equilibrium liquids. Now that these problems have been solved and present computers are able to handle continuous potentials efficiently, interest in the hard-sphere and square-well problems has abated somewhat.
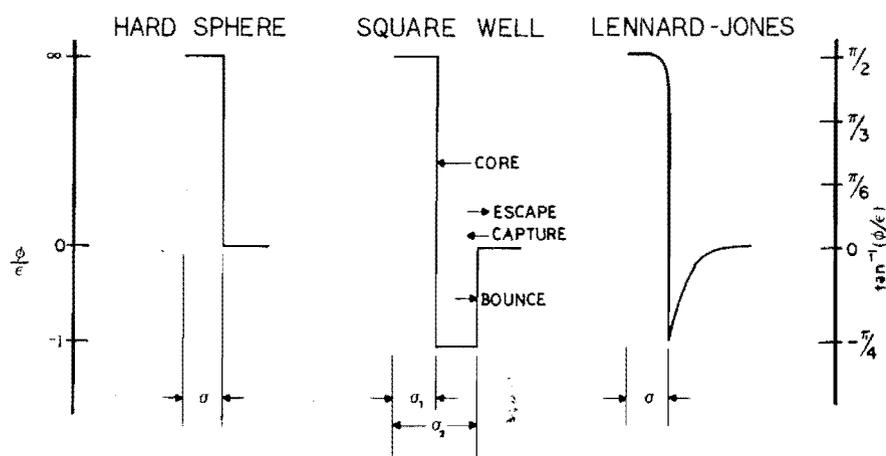
Fig. 4. Hard-sphere, square-well, and Lennard-Jones pair potentials. Each has been used extensively in molecular dynamics calculations.

D. LIMITATIONS

Molecular dynamics calculations are limited in scope, accuracy, and trajectory length by the computer time required to calculate the interparticle forces. If all of the $N(N-1)/2$ force components are explicitly calculated, then the maximum time interval that could be studied in 10^4 sec of computer time would be of order

$$10^4 \times 10^7 \times dt/N^2$$

if we make the optimistic assumption that 10^7 force components per second can be calculated. For argon at its triple point, dt is 10^{-14} sec—larger values lead to excessive energy-conservation errors. Thus 864 argon atoms could be (and have been) followed in time for about one nanosecond. A slight improvement over such estimates results if a table of near neighbors, revised occasionally, is maintained while carrying out the calculation. The force contributions between faraway pairs of particles can then be ignored. This improvement can increase the maximum trajectory lengths by roughly one order of magnitude.

A second possibility for studying longer trajectories is applicable to plasmas or to astrophysical systems. In either case the pair potential is long range ($\propto 1/r$), and the particle motion is influenced primarily by faraway neighbors rather than close ones. The effect of the far neighbors can be approximated by dividing space into a number of zones and calculating a field by counting the number of particles per zone ignoring the precise locations. This simplification makes it possible to study some tens of thousands of particles in astrophysical problems (Hohl, 1972).

Because the computer simulation is limited to short times, functions whose relaxation time is of order 1 nsec or more cannot be accurately determined in computer calculations. It is for this reason that the only thermodynamic functions normally measured are the pressure, potential and kinetic energies, and their fluctuations. Higher order fluctuations require prohibitively large computer runs. The time required to dissipate a temperature fluctuation in an 864-atom simulation of argon at its triple point can be estimated from the thermal diffusivity, 8×10^{-4} cm^2/sec, and the system half-width, 3.4×10^{-7} cm: $(3.4 \times 10^{-7})^2/(8 \times 10^{-4}) = 10^{-10}$ sec, close to the maximum time such a system can be studied. The decay of higher fluctuations (specific heat fluctuations, for instance) is driven much more weakly and requires longer times.

Both the study of particle trajectories and the study of thermodynamic functions suggest that in numerical work it is better to estimate several values of low-order derivatives than fewer values of high-order derivatives. It

would be interesting to have a quantitative study analyzing the time-dependence of the high-order derivatives for a simple system (such as a Boltzmann-limit gas) in order to make these statements more precise.

In addition to limitations imposed by relaxation times, the finite size of systems limits the length scale of the phenomena to be studied. A very "large" computer system of 16,384 particles, is, for triple-point argon, only 87 Å in width. Many interesting problems with "small" characteristic lengths are still too large for efficient computer study. Turbulence, for example, has characteristic lengths of the order of 1 mm. Fracture, which is dominated by dislocations, voids, and grain boundaries, is another example of a small-scale phenomenon too large for effective study on the atomic scale. Although these two problems are too large-scale for comprehensive simulation, their salient features—viscosity, dislocation motion, void growth, and grain boundary structure—*can* be individually treated.

Fortunately many thermodynamic and hydrodynamic properties are relatively insensitive to long-wavelength phenomena. When periodic boundaries are used, errors in equilibrium properties due to the finite size of computer systems are typically of order $1/N$ or $\ln N/N$. The insensitivity of transport properties to system size is not so well characterized. As we will see, errors of order $N^{-1/3}$ can occur.

E. Nonequilibrium Boundary Conditions

Nonequilibrium conditions can be established, or maintained, in three distinct ways: (i) initial conditions deviating from the normal equilibrium range, allowing the approach to equilibrium to be studied; (ii) interaction with an external field that acts upon all of the particles in the system; or (iii) interaction with an external field that acts only on some of the particles, such as those sufficiently close to a boundary of the system. All three kinds of nonequilibrium systems have been studied. The first kind involves the decay of an isolated system rather than a steady process such as heat flow between boundaries of different temperatures. The other two kinds of system can be used to study either steady or nonsteady nonequilibrium problems.

Because nonequilibrium systems dissipate work (or available work, such as chemical potential) into heat (or entropy, such as the entropy of mixing) any steady state problem must include a means for removing thermal energy (or particles) from the system. This is most easily achieved by the approach in which thermal reservoirs are maintained along the boundary (Ashurst, 1974). It would be possible to use a complicated external field (analogous to Maxwell's demon) to extract heat throughout a system, not just at the boundary. Although this method would have the advantage of reducing

boundary effects, it has the very real disadvantage of altering the nonlinear properties of the "bulk" system being studied.

If the third approach is adopted, in which only some of the particles interact with external forces, the exact form of these forces has to be chosen judiciously to minimize the effects of the boundary on the bulk material. It is well known from equilibrium work that boundary effects produce changes in the intensive bulk properties of order $N^{-1/3}$ (the surface-to-volume ratio). Even for a large 1000-particle system these effects are of order 10%. To minimize boundary effects a boundary region, such as that shown in Fig. 5,
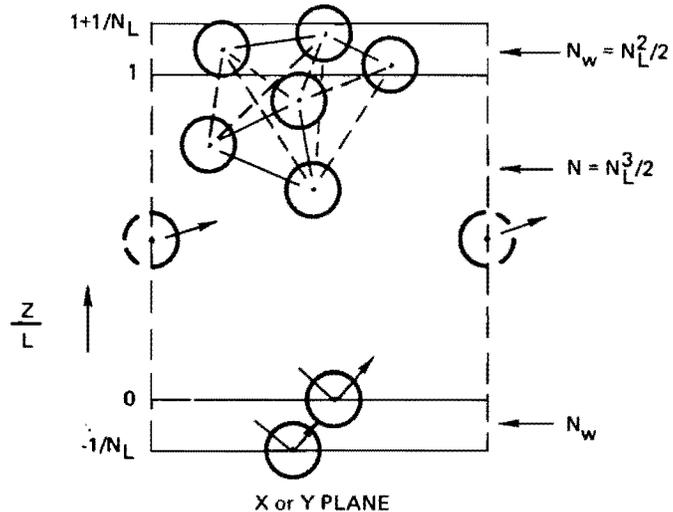
Fig. 5. Boundary conditions used in computer simulation of momentum or energy flow. The upper and lower regions contain N_w particles each, confined by reflecting elastic walls (the other two directions have periodic boundaries). The central region, within which fluxes are measured, contains N particles. The velocity and temperature of the upper and lower regions are maintained by the use of external momentum and energy reservoirs.

can be used. Provided that this region has a thickness comparable to the range of the interparticle forces, particles near the boundary will behave very much like those in the bulk, surrounded in all directions by homogeneous fluid. From the operational viewpoint, the boundaries should be adjusted to simulate an infinite half-space of material as closely as possible.

An unfortunate aspect of most useful boundary conditions is that it is not yet clear how to treat their effects theoretically. The conventional Fourier analysis (in both space and time) of the mass density, momentum density, and energy density fields seems not to be closely related to the boundary-value problems found in physical simulations.

In the next two sections we consider some of the specific results that have been obtained using the three kinds of nonequilibrium methods just described.

III. Nonsteady Problems

A. Approach to Equilibrium

What is a nonequilibrium system? This question is not easily answered in general because it depends upon both the scale of observation and on the number of variables used to describe the system of interest. Nonequilibrium systems must have at least one measurable property that lies outside a "reasonable" equilibrium range. The property in question could be an element of the pressure tensor, a Fourier component of the density or temperature, in fact *any* of the variables that are free to fluctuate at equilibrium. In an isolated system if any such variable somehow attains, or is given, an initial value outside the normal range, this variable will relax toward its equilibrium value, and, to the extent that this relaxation can be *reproducibly* characterized, a nonequilibrium description of that relaxation is both possible and interesting. On the other hand, if the deviation from equilibrium is small, then a reproducible approach to equilibrium is *not* exhibited. Such *fluctuations* are themselves not normally of much interest in a macroscopic description. We want to describe and characterize the predictable *similarities*, rather than the randomly fluctuating *differences* among nonequilibrium systems. Despite the lack of intrinsic interest in *small* fluctuations, we will see that these *do* play an important role in the Green–Kubo formulation of the transport coefficients discussed later in this section.

B. Hard Spheres

In 1955 Alder and Wainwright studied the relaxation of a nonequilibrium system of hard spheres from an unlikely initial condition—all of the spheres had identical speeds but the velocity directions were chosen randomly so that the initial velocity distribution was a single spherical shell in $v_x v_y v_z$ space (Alder and Wainwright, 1958). The study was carried out with periodic boundaries, to eliminate surface effects, and at low density, to eliminate particle correlations. Under these conditions the Boltzmann equation should provide a nearly correct description of the change in the velocity distribution $f(|\mathbf{v}|)$ with time:

$$df/dt = (\partial f/\partial t)_{\text{collisions}} \tag{9}$$

where $f \, d\mathbf{r} \, d\mathbf{v}$ is the number of particles in $d\mathbf{r}$ (the total volume V in this case) and $d\mathbf{v}$ (a spherical shell of volume $4\pi v^2 \, dv$ in this case). The collision term, not written explicitly, is an integral, quadratic in f because two particles participate in each collision. The collision integral is formulated as a two-body integral rather than an N-body integral by ignoring all interparticle correlations.

Within the statistical accuracy of the results (ignoring the fluctuations present due to the small size of the system studied, $N = 100$) the Boltzmann equation predicted quantitatively the initial decay toward a Maxwell–Boltzmann (gaussian) velocity distribution. This instructive example showed that, apart from fluctuations, the Boltzmann equation *does* describe the low-density approach to equilibrium. Because no diffusion processes were involved, the approach to equilibrium was very rapid, taking on the order of three collisions per particle to reproduce the low- and moderate-velocity parts of the equilibrium velocity distribution.

As equilibrium was approached, Boltzmann's H function ($\langle \ln f \rangle$, which is the velocity average of $\ln f$) was approximated by histogram integration as a function of time. Boltzmann's analog of the second law of thermodynamics, the H theorem, states that $\langle \ln f \rangle$ will decay monotonically to its equilibrium value. The theorem is consistent with the idea that H, apart from known additive and multiplicative constants, is the negative of the thermodynamic entropy. In Alder and Wainwright's calculation H did decay monotonically until it reached the level of equilibrium fluctuations.

The example points out the usefulness of hydrodynamics in following decays, and also shows that a different theory, equilibrium fluctuation theory, has to be used once the decay is complete.

C. Nearly Harmonic Oscillators

Because an isolated system of coupled harmonic oscillators cannot ever reach equilibrium (because the energy in each mode of the system remains constant), it is plausible that even when coupled oscillator systems are slightly anharmonic they still cannot reach equilibrium. At the same time, an optimist might hope that small anharmonic perturbations (cubic or quartic terms in the lattice potential, expanded in powers of the particle displacements) would *eventually* drive the oscillators to equilibrium. Tests of one-dimensional coupled particles joined by anharmonic springs were run on Los Alamos' Maniac computer by Fermi *et al.* (1955). The results were quite interesting. The top portion of Fig. 6 is a time-history of the energy residing in the first four excited modes of a 16-particle chain. Initially all of the energy was in the lowest-frequency mode 1. After about 13,000 time steps the amplitude of that mode had recovered from a substantial decay into modes 2, 3, and 4, and the initial conditions were nearly (but not quite!) reproduced. Fermi *et al.* could conclude at least that equilibrium is not achieved rapidly. The results certainly suggest that equilibrium might *never* be achieved. The problem aroused interest and considerable discussion. After several years had passed Tuck and Menzel (1972), armed with a faster and more accurate computer, reinvestigated the problem. A portion of their investigation,
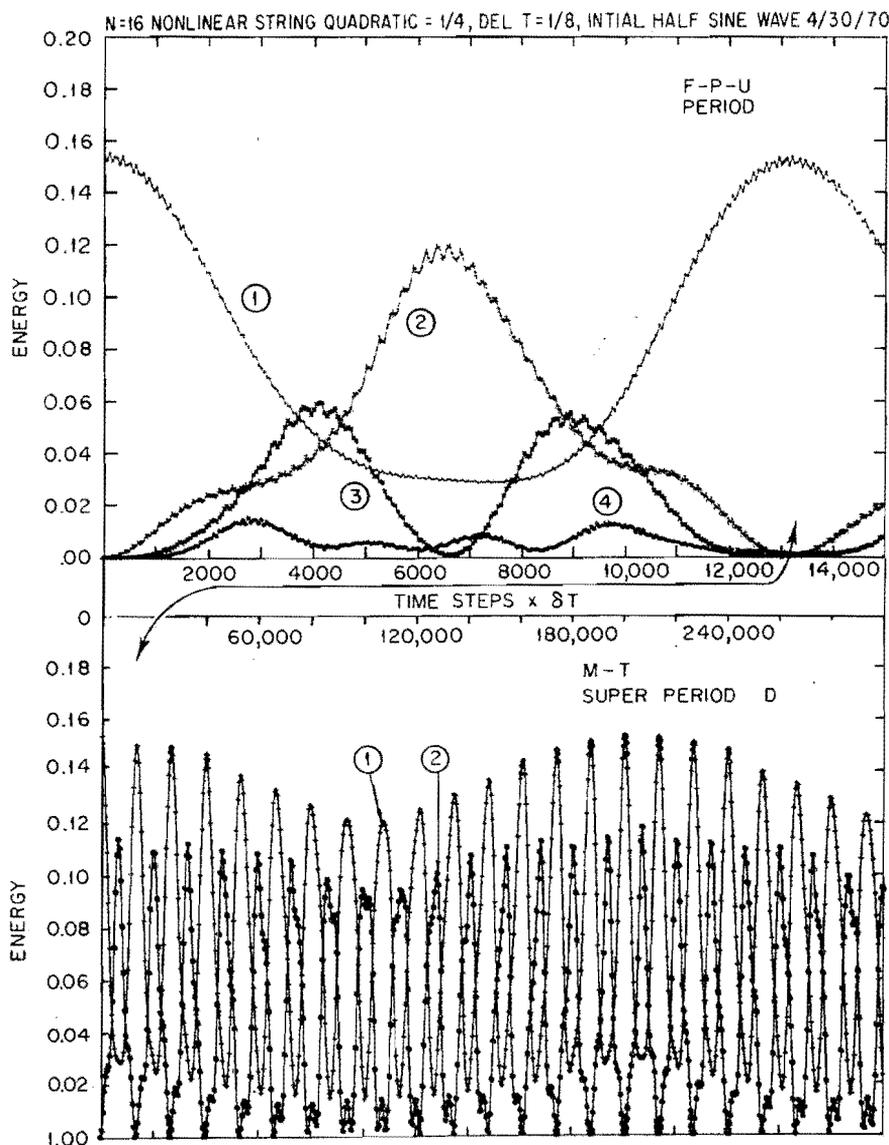
Fig. 6. The upper figure recalculates the Fermi-Pasta-Ulam result

$$\ddot{x} = (x_{i+1} - x_i) - (x_i - x_{i-1}) + \alpha(x_{i+1} - x_i)^2 - \alpha(x_i - x_{i-1})^2$$

for 16 particles with $\alpha = \frac{1}{4}$. (1) = fundamental; (2) = second harmonic, etc. The fundamental period τ_0 is 32 ($= 256 \ dt$). The Fermi-Pasta-Ulam period is $51.69\tau_0$. The lower figure continues the calculation for longer times to reveal the superperiod $840\tau_0$. Fraction of initial total energy returning to the fundamental: 0.993 at the Fermi-Pasta-Ulam period; 0.99993 at the Tuck-Menzel period. From Tuck and Menzel (1972).

covering 22 near repetitions of the initial condition, is shown at the bottom of Fig. 6. The long calculation showed that the energy amplitude in mode 1 at first gradually decreased, from maximum to maximum, perhaps illustrating a lethargic approach to equilibrium. Tuck and Menzel, however, soon

discovered a "superperiod." After the eighth decreasing near-repetition of the initial condition, each time with a slightly lower energy peak, the energy peaks in mode 1 began to rise again, approaching very near (within 0.007%) the initial value at the fifteenth near-repetition. This example illustrates that it is possible to find systems which really *are* pathological (i.e., contrary to ordinary experience).

In a mathematical sense, the pathology is now understood. Subsequent theoretical work showed that there is a *threshold* for irreversible behavior. Unless the anharmonic part of the energy is sufficiently large, a nearly harmonic system will undergo the quasi-periodic motions illustrated by the nearly harmonic Fermi–Pasta–Ulam problem. It has also been shown that the completely anharmonic hard-sphere system does achieve equilibrium. The crucial physical property underlying this behavior is the instability to small trajectory perturbations—the same phenomenon that destroys reversibility in the computer experiments. For a recent discussion of work on the approach to equilibrium, which is still being actively pursued for two-dimensional anharmonic systems, the interested reader should consult Ford's review (1973).

D. Green–Kubo Relations

The Green–Kubo relations link the phenomenological linear transport coefficients of hydrodynamics to the decay of equilibrium fluctuations—in this sense the Green–Kubo relations are based upon an ensemble-averaged approach to equilibrium. The several derivations summarized in Zwanzig's excellent review (1965), together with the more physical treatments of Helfand (1960) and Gass (1969), all lead to the same conclusion: the diffusion of mass, momentum, and energy can be described by linear laws with coefficients of diffusion, viscosity, and thermal conductivity which are proportional to autocorrelation integrals of the mass, momentum, and energy fluxes. Shear viscosity, for example, describes the way in which x momentum diffuses in the y direction. The shear viscosity coefficient η can be determined by evaluating the ensemble-averaged decay of the xy component of the pressure tensor (the ij component of the pressure tensor is the flux of i momentum in the j direction):

$$\eta = \frac{V}{kT} \int_0^\infty \langle P_{xy}(0)P_{xy}(t) \rangle \, dt. \tag{10}$$

The compact representations of transport coefficients in terms of equilibrium fluctuations owe their origin primarily to Green (1952) and Kubo (1957). With fast computers it is possible to measure the averaged decay of equilibrium fluctuations and thereby to determine the transport coefficients.

Before discussing the results obtained from the Green–Kubo relations it is important to emphasize that their use involves the usual assumption that finite-system computer calculations, carried out for a short time, give results sufficiently close to the large-system long-time limits of thermodynamics and hydrodynamics. We expect, for example, that local anomalies in mass, momentum, or energy will eventually diffuse away according to the laws of hydrodynamics, at least on the average (i.e., ignoring fluctuations). Thus an initial perturbation is smeared out by diffusion over a half-width of order $\text{time}^{1/2}$; the amplitude of the perturbation is thus of order $\text{time}^{-D/2}$ in a D-dimensional system. The suggestion that the Green–Kubo integrands decay in this way has been predicted theoretically and is supported by computer studies (Alder, 1973; Levesque and Ashurst, 1974). For two dimensions, heuristic arguments suggest that the long-time decay may be of order $(t^2 \ln t)^{-1/2}$ rather than $1/t$, but the presence of a $(\ln t)^{-1/2}$ correction would be difficult to confirm numerically (Visscher, 1973).

The long-time hydrodynamic analysis of the Green–Kubo integrands suggests that transport coefficients *diverge* in two-dimensional systems. It is essential, if transport theory is to be understood, to uncover the size- and time-dependence of this divergence and its physical meaning, if any. It seems likely (Hoover *et al.*, 1974) that two-dimensional transport coefficients depend weakly on system size and are not otherwise anomalous.

For three-dimensional systems, the convergence of the Green–Kubo integrals is slow but sure. The hard-sphere transport coefficients were determined over the whole fluid density range by Alder *et al.* (1970). The results showed that the simple Enskog model (Hirschfelder *et al.*, 1954), which takes into account the density enhancement of the collision and transport rates at high density, but ignores the effect of collision correlations, reproduces the density dependence of the transport coefficients fairly well. At the freezing point the measured diffusion coefficient from mass-flux decay is about half the Enskog-model prediction and the shear viscosity is twice the Enskog prediction. At lower densities the errors are smaller. The hard-sphere results have proved useful in predicting transport coefficients for other, more complicated potentials (Levesque *et al.*, 1973).

Green–Kubo calculations of the transport coefficients for the more realistic Lennard-Jones potential

$$\phi = 4\varepsilon[(\sigma/r)^{12} - (\sigma/r)^6] \tag{11}$$

were carried out by Levesque *et al.* (1973) using 864 particles chosen to simulate liquid argon near its triple point. For argon, the run duration corresponds to 1 nsec. The resulting shear viscosity is 30% larger than the experimental argon value (this disagreement is three times the uncertainty in

the calculated value). The calculated thermal conductivity is about twice the experimental value and the calculated bulk viscosity is half the experimental value. How can these disagreements be understood? Of course, the Lennard-Jones potential is not a perfect representation of the interparticle interaction in liquid argon. However, this effective potential *does* reproduce the energy and the pressure for argon quite well. Thus, it is hard to understand a factor-of-two discrepancy in the energy transport. A study of the number-dependence of these results, using systems of smaller size (larger ones are too expensive at present), might be useful, as is the comparison of these results with those obtained more directly, without the use of the Green–Kubo theory, as is discussed in Section IV.

E. RADIATION DAMAGE SIMULATION

The first large-scale computer experiments using realistic potentials were the solid-phase studies of Vineyard and his collaborators (Gibson *et al.*, 1960). This work sought to understand the interaction of fast neutrons with metals, an important problem underlying reactor design. Because neutron free paths are long, of macroscopic length, their slowing down can be treated as a series of infrequent collisions with metal atoms. Each collision leads to localized regions of "damage" (vacancies and interstitial atoms) around the initial collision site. These damaged regions, for energies up to a few hundred electron volts, are small enough to be studied with nonequilibrium molecular dynamics.

The atoms are treated as point masses interacting with simple pairwise-additive potentials. These potentials are chosen to reproduce macroscopic parameters such as the molar volume, binding energy, and elastic constants. Electrons are not explicitly treated—this is probably the only serious approximation made in the calculations.

Initially a finite three-dimensional lattice of atoms is excited by giving an impulse to a single atom, simulating a neutron collision; then the equations of motion are solved to generate the resulting "cascade" of mass, momentum, and energy redistribution.

The crystal boundary conditions are important in these calculations because lattice relaxation times exceed the sound-traversal time for these small crystals. Simple periodic boundaries would distort the results by allowing an outgoing sound wave, produced at the collision site, to reenter on the opposite side rather than dissipating in fresh material surrounding the damaged region. To avoid this reentry and make it possible to follow these systems for longer times in a realistic way, Vineyard's group developed a set of boundary conditions designed to simulate an infinite surrounding elastic continuum with 500 or 1000 discrete particles inside. The outermost discrete particles

interact with external viscoelastic forces in such a way as to simulate the response of an infinite crystal. The elastic constants restoring displaced particles toward their lattice sites are chosen to match the displacement characteristics of a macroscopic region within an infinite elastic continuum. The spring constants acting on the boundary particles turn out to be much smaller than interparticle spring constants. This is a consequence of the lattice relaxation which occurs in the vicinity of a displaced region in a macroscopic continuum.

Since a perfectly elastic boundary has no kinetic energy, elastic boundaries would reflect any incident waves, leading to the same interference problems as in the periodic case. The unwanted reflection can be minimized by adding viscous damping forces to the boundary particles with longitudinal and transverse viscosities chosen to absorb, rather than reflect, incident waves as well as possible. Even with the optimal choices of viscosity, some of the energy is reflected and incident energies have to be limited to a few hundred eV.

The calculations have recently been summarized by Vineyard (1972). Some of the interesting phenomena studied are:

(i) Determination of the threshold energy, as a function of direction, for permanent radiation damage and correlation of the number of interstitial–vacancy pairs created as a function of energy.

(ii) Stability of the defects formed. Certain kinds of defects, including some predicted to exist in theoretical studies, were found to be unstable. In Fig. 7 the region within which an interstitial and a void can recombine in irradiated copper is indicated. The figure shows that in the 110 direction the distance between the defects must exceed three lattice spacings in order to avoid self-annealing annihilation of the two defects.

(iii) Focusing, in which mass, momentum, and energy are transferred through the lattice in highly preferred directions, was studied. An unexpected result of the pioneering calculations on copper (Gibson *et al.*, 1960) was the strong focusing occurring in the 100 direction, in which the nearest-neighbor spacing is relatively large. The mechanism involves the cooperative motion of particles in four neighboring parallel rows.

One of the major problems encountered with fast computers able to solve problems in *three* space dimensions, not just one or two, is displaying the results. It is not unusual for the programming time and ingenuity devoted to the display aspect of the problem results to exceed the effort of generating the original data. Portraying the radiation damage just discussed is one example of a challenging programming task. Figure 8, based on a 5-kV collision in iron (Beeler, 1966), gives a graphic portrayal of the extent of damage to the crystal.

Fig. 7. Stability of vacancy-interstitial pairs in a computer simulation of radiation damage to copper. The line separates sites at which a vacancy is stable from sites at which a vacancy will spontaneously combine with the interstitial atom shown at the center of the figure. From Gibson *et al.* (1960).

The radiation damage is important historically as an early use of continuous potentials in nonequilibrium molecular dynamics. Vineyard's work also sets a high standard in clarity and breadth and suggests a useful treatment of nonequilibrium boundaries. We anticipate that related calculations, for even more complicated defect structures, will appear with increasing frequency in the future.

F. STAR-CLUSTER EVOLUTION

An isothermal classical system with purely attractive pairwise-additive forces can have no extensive thermodynamic properties. The energy, for example, if it does not diverge, is at least proportional to N^2 rather than to N. This unusual behavior makes it interesting to speculate on the peculiar physical characteristics of a system with attractive forces only. Stellar dynamics furnishes many examples. Astronomical bodies attract one another with inverse-square gravitational forces. Thus a system of stars, in "equilibrium" with a heat reservoir, should eventually collapse into a compact

Fig. 8. Perspective view of a damaged region in a computer simulation of radiation damage in α-iron. The initial energy responsible for the damage was 5 keV. From work by J. R. Beeler, Jr., cited by Vineyard (1972).

cluster of particles with an energy approaching minus infinity. If no heat reservoir were present, to absorb the gravitational energy, what would happen? The answer is not known for certain, but recent simulations of star clusters strongly suggest (Aarseth, 1972) that a cluster of stars will gradually contract, lowering the potential energy. This energy drop is compensated for by an increase in kinetic energy, with an occasional spectacular high-speed escape of a star that has acquired, through collisions with its neighbors, enough kinetic energy to escape the gravitational field of the other stars.

Computer simulation of astrophysical systems began over 10 years ago (Contopoulos, 1966) and is still a rapidly expanding field (Lecar, 1972). Simulations of star clusters reveal the ubiquitous appearance and persistence of a tight binary double star near the center of the cluster. It appears that this binary cluster approaches minus infinity in energy while supplying sufficient energy to the other stars to make their escapes possible. The rather interesting spectacle of a gradual explosion of the cluster, as opposed to a collapse, ending up with $N - 2$ high-speed isolated stars and a tightly bound binary star, would probably not have been postulated without the help of nonequilibrium molecular dynamics.

IV. Steady State Problems

The simplest possible nonequilibrium systems are macroscopically steady, not changing with time. To obtain more accurate steady state values (at fixed size) simply means extending the observation time of the computer experiment. In nonsteady problems several repetitions of a calculation, with slightly different initial conditions, would have to be carried out to reduce the fluctuations in the hydrodynamic variables. In the nonsteady case the significance of this averaging over different initial conditions is not clear.

These nonequilibrium systems must dissipate work into heat, which distinguishes them from equilibrium systems. Thus, external forces either do work and extract heat *or* replenish chemical potential and extract entropy in order to maintain fixed hydrodynamic boundary conditions. The external forces may act throughout the system *or* be restricted to special boundary regions. The shear viscosity coefficient for dense fluids has been recently calculated by both methods and the thermal conductivity coefficient by the latter method. We will present the details of our calculations in this section.

A different type of nonequilibrium system is a sound or shock wave, which, when viewed in a coordinate system fixed with respect to the wave front, becomes a steady state system connecting two equilibrium systems at different conditions. The shockwave problem has been studied (Paskin and Dienes, 1972; Tsai and Beckett, 1966), but due to constraints implied by the finite width of the systems treated, it is premature to draw firm conclusions from this work. Some solutions of the shockwave problem at zero density are available from the statistical viewpoint of the Boltzmann equation (Bird, 1970). Another type of nonequilibrium system could be one created by the notorious Maxwell demon (i.e., a nonzero steady state flux is maintained by labeling mass, momentum, or energy without affecting the equilibrium system). This approach was recently used by Holian for calculating self-diffusion and will be described next. We expect that in the near future a growing variety of steady state problems will be solved.

A. Diffusion

Diffusion in a periodic *equilibrium* system of hard spheres has recently been studied by Holian *et al.* (1973, private communication of BLH to WGH) using the artifice of coloring particles according to their most recent crossing of a plane (i.e., the Maxwell demon has a paint brush). The use of periodic boundaries minimizes the surface effects inherent in most nonequilibrium problems. All particles crossing the plane $z = L/2$ in the upward (downward) direction, for example, could be colored red (white). After a time the result of this coloring process is to produce two opposing concen-

tration gradients, one white and one red, which result in, or coexist with, opposing fluxes of the colored particles. It is not particularly obvious just how linear the concentration profile will be. In fact, the numerical work indicates a profile linear within 1% fluctuations, except very near the concentration discontinuity induced by the coloring plane.

To improve the accuracy of the results, Holian *et al.* (1973, private communication) colored the particles independently for each of the three directions x, y, and z. They also confirmed that the diffusion coefficients found from Fick's law, $D = -j_z (dz/d\rho)$, were independent of the fraction of particles colored, for fractions 0.2, 0.4, 0.6, 0.8, and 1.0. The results found by this direct method are shown in Table I along with those derived from the Green–Kubo relation at the same density and temperature and for the same number of particles by Alder *et al.* (1970).

Table I

DIFFUSION COEFFICIENTS FOR 108, 500, AND 4000 THREE-DIMENSIONAL CLASSICAL HARD SPHERES IN FINITE PERIODIC SYSTEMS[a]

	D/D_E	
N	Alder *et al.*	Holian *et al.*
108	1.16	1.17
500	1.22	1.23
4000		1.29

[a] The density is one-third the close-packed density. The diffusion coefficients have been divided by the prediction of the Enskog model, $D_E = 0.219\sigma(kT/m)^{1/2}$. The uncertainty in the computed coefficients is about 1%. The calculations involve on the order of a million collisions each.

An important problem waiting to be solved is the generalization of the work of Holian *et al.* to the transport of momentum and energy. In either of these cases, the labeled flows of conserved quantities, divided by the appropriate gradient, would determine the corresponding viscosity or conductivity coefficient. The attractive aspect of such a method would be that an undisturbed equilibrium system becomes the "nonequilibrium" system with the entropy of mixing acting as the driving force to maintain the steady state flux.

B. Shear Viscosity

Viscosity describes the momentum diffusion responsible for broadening a propagating pressure pulse. For example, an initial localized pulse of x momentum spreads out in the y and z directions with a half-width of order $(\eta t/m\rho)^{1/2}$ for long times, where η is the shear viscosity and ρ is the number density. Eventually viscosity annihilates velocity gradients and converts their kinetic energy into heat. The local rate of heat production, or "power density," is proportional to the viscosity coefficient and the square of the gradient, for small gradients:

$$\lambda(\nabla \cdot \mathbf{v})^2 + \tfrac{1}{2}\eta(\nabla\mathbf{v} + \nabla\mathbf{v}^\dagger):(\nabla\mathbf{v} + \nabla\mathbf{v}^\dagger),$$

where λ and η are the Newtonian viscosity coefficients:

$$\mathbf{P} = [P_0 - \lambda(\nabla \cdot \mathbf{v})]\mathbf{I} - \eta(\nabla\mathbf{v} + \nabla\mathbf{v}^\dagger). \tag{12}$$

The heat produced by viscous dissipation has to be conducted away or absorbed in any "steady" calculation, so that any such viscosity study must also include a mechanism for heat absorption.

For shear viscosity determination, a possible homogeneous system can be created by using external forces to shear a periodic system, each particle being given, at every time step, an additional x displacement proportional to its y coordinate. These displacements can actually be added in at every time step or, alternatively, a coordinate system with changing oblique coordinate axes can be used. For the former method, a particle's periodic image above (below) the basic cell is shifted in the positive (negative) x direction by γLt; where γ is the shear rate, L is the y distance between images, and t is the current time (see Fig. 9). Hence for this special periodic boundary, when a particle leaves a y face it enters the opposite face with a shifted x coordinate. The heat generated by this external shear force can be eliminated by a thermostat which rescales the particle velocities at each time step. Earlier exploratory work along these lines was carried out by Lees and Edwards (1972). Some recent more-accurate results we have obtained using this method are shown in Figs. 12 and 18.

The method just described resembles a novel shear viscosity determination carried out by imposing an external sinusoidal force field on a periodic fluid system, with the x field component proportional to $\sin(2\pi y/L)$. The amplitude of the resulting sinusoidal velocity profile can be related to the viscosity coefficient (Gosling *et al.*, 1973). Because these sinusoidal-force calculations contained no provision for extracting heat, the dynamical history was not actually steady, but increased gradually in temperature as the runs continued. The homogeneous shear discussed above has the advantage of eliminating the relatively short wavelength character of the velocity
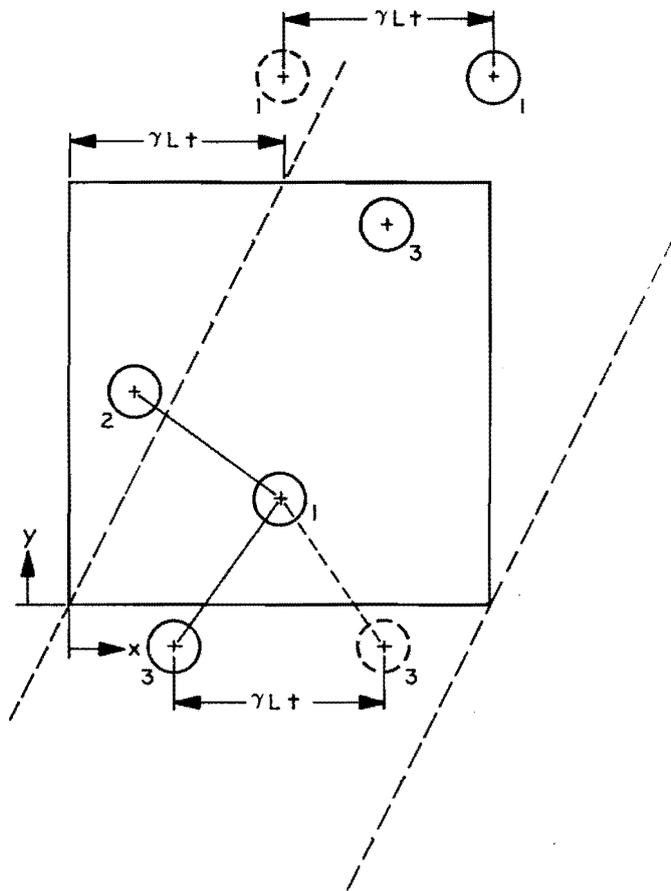
Fig. 9. Steady homogeneous shear system at time t with shear rate γ. The particle's periodic image is displaced by γLt from the conventional periodic image (shown by dash line).

field, producing results closer to the large-system hydrodynamic limit. However, since the external force field acts upon all the particles, the nonlinear properties are somewhat altered from those in a nonequilibrium system free of external forces; see Fig. 18.

In order to create a nonequilibrium system with a bulk region free of external forces, special boundary regions have been developed to maintain the desired hydrodynamic values (e.g., density, flow velocity, and temperature) which will produce a steady state flux of momentum or energy (see Section II and Fig. 5). The time-dependent external force in the boundary region is the negative of the force interaction between the bulk fluid and that boundary region. This total external force is divided equally among the boundary region particles and thus constrains only the region's mean flow velocity; i.e., the external force acts as a momentum reservoir. Velocity scaling, adjusting the second moment with respect to the mean at each time step, plays the role of a heat reservoir. To maintain the number density, the planes separating the boundary regions from the bulk fluid reflect the occa-

sional particles that attempt to leave either region. This method based on special boundary regions has been used to simulate shear flow of relatively dense nonideal two- and three-dimensional fluids (Ashurst, 1974; Hoover *et al.*, 1974; Ashurst and Hoover, 1973).

From the resulting simulation of nonequilibrium flow, the shear viscosity can be determined from either a microscopic or a macroscopic viewpoint. The microscopic pressure tensor component P_{xy} depends on particle velocities and coordinates:

$$P_{xy} V = \Sigma m v_x v_y + \Sigma - xy\phi'/r; \qquad (13)$$

a time-average of P_{xy} together with the average shear rate dv_x/dy determines the linear or newtonian shear viscosity η. Alternatively the macroscopic hydrodynamic work done (or heat extracted) can be set equal to the product of the viscosity coefficient, the velocity gradient, the surface area, and the relative displacement of the two boundary planes. Agreement of the two methods serves as a consistency check on the calculation. However it is necessary to determine the velocity gradient within the system since the boundary region is not perfectly coupled and there is some velocity slip. Thus local values of the velocity and temperature gradient have to be determined and related to the hydrodynamic flow solution. These difficulties can be avoided by using a homogeneous shear system without special boundary regions.

How *does* one generalize small-system results to systems of macroscopic size? When periodic boundaries are used, finite size equilibrium systems have errors of order $1/N$ or $\ln N/N$. For nonequilibrium systems, several kinds of extrapolation have to be carried out. The number of particles should be large; the gradient should be small, and the boundary influence should be minimized and corrected for. An immediate problem in the computer experiments is that the large-system and small-gradient limits cannot be realized. Computer speed limits the size and statistical fluctuations can mask small-gradient effects.

In addition to the size and gradient limits, three other criteria should be considered. The flow should be laminar, not turbulent; steady, not fluctuating; and isothermal, so that a well-defined thermodynamic state is being investigated. The restriction to laminar flow means, macroscopically, that fluctuations in the flow are small. Large-scale macroscopic fluctuations in flow, called "turbulence," occur whenever the viscous forces are too small to damp out naturally occurring velocity gradients. On the microscopic level it seems more natural to consider the flow of momentum as being well defined in the event that it exceeds the natural fluctuations in the flow. In either case a steady nonequilibrium system can be studied only if the steady behavior can be distinguished over the nonsteady perturbations.
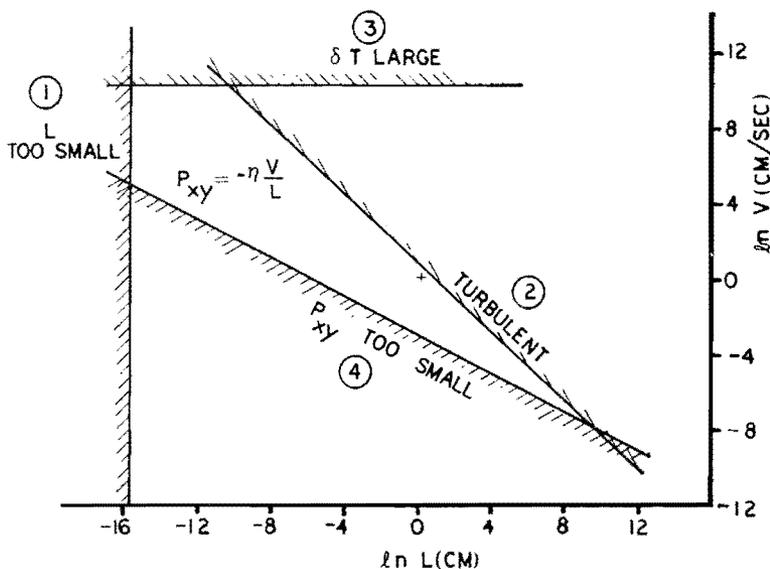
Fig. 10. Limitations on the sidelength L and relative velocity v for a cube of triplepoint argon undergoing plane Couette flow. Line 1 indicates that the volume element size must exceed atomic dimensions; line 2 separates the regions of laminar and turbulent flow; line 3 separates the regions of large and small temperature gradients resulting from the shear flow; line 4 separates the regions in which the shear stress is large or small relative to pressure fluctuations. In the central quadrilateral the motion of the volume element can be usefully described by macroscopic hydrodynamics.

In Fig. 10 we plot, for argon at its triple point, the region in velocity–size space to which viscosity measurements are limited. The four different boundary lines shown in that plane separate qualitatively different regions for a cubical volume element with sidelength L and a velocity difference v between its upper and lower walls. The lines shown are as follows:

Line 1 indicates that L must exceed atomic dimensions.

Line 2 indicates that the flow must be laminar rather than turbulent. The Reynolds number criterion for turbulent flow is $\text{Re} = vLm\rho/\eta > 3000$ (Schlichting, 1960).

Line 3 indicates that the boundary temperature should differ from the central temperature by no more than 10%. (This restriction effectively forces v to be less than typical thermal velocities.)

Line 4 indicates that the shear stress induced by the velocity gradient v/L must exceed the momentum flux fluctuations ($\sim N^{1/2}kT/L^3$).

Each of the lines just constructed forms a part of the boundary of the region within which viscosity is important in characterizing the pressure tensor. By using low velocities a system width of 1 mm can be achieved, large enough so that boundary details are unimportant. In nonequilibrium molecular dynamic calculations we are restricted to much smaller systems and hence

larger velocities. The widest system studied so far is 50 Å in width with velocity difference of $(kT/m)^{1/2}/8$.

1. Soft-Sphere Potential

In order to test the steady nonequilibrium molecular dynamic method just described, the soft-sphere potential

$$\phi(r) = \varepsilon(s/r)^{12} \tag{14}$$

was chosen for exploratory work. The equilibrium thermodynamic properties for systems composed of soft spheres have already been characterized (Hoover *et al.*, 1970). The lack of attractive forces eliminates the complications caused by gas–liquid density fluctuations. A single fluid phase extends from zero density to the freezing point density, which is $Ns^3/\sqrt{2}\,V = 0.813(kT/\varepsilon)^{1/4}$.

Because computer time involved in nonequilibrium problems is typically a few hours, and increases more rapidly than linearly with the number of particles, it is desirable to use the smallest possible system capable of providing accurate results. To identify this minimum size, three different system sizes, $N = 32$, 108, and 256 (plus boundary particles), were investigated at three-fourths the freezing density. Each of the three systems was run for the time required to displace the upper boundary-region particles 16 system lengths relative to the lower boundary-region particles with a velocity difference between the regions of $(kT/m)^{1/2}$. The averaged velocity profiles, obtained by dividing each system into ten equal spatial regions, are shown in Fig. 11. Despite the relatively long run the 32-particle velocity profile shows deviations from the expected linear profile. We conclude that with the present choice of boundary regions, 108 particles, or more, are required for quantitative work.

For a given system size at fixed density and boundary temperature, the results may depend upon the relative velocity of the two boundary regions, i.e., shear rate. In order to test this dependence, a range of relative wall velocities [all of order of the thermal velocity $(kT/m)^{1/2}$] was examined at four dense-fluid densities. The results are listed in Table II and displayed in Fig. 12. The data indicate no significant number-dependence at a reduced density of 0.6, where most of the runs were made. There *is* a definite *increase* in viscosity with decreasing shear rate. Corresponding results from the homogeneous shear method (external forces *throughout* the system maintain the shear flow) are also shown in Fig. 12 (flagged circles). The two methods have reasonable agreement. However, it is not certain that the two methods will agree for low density. The kinetic or streaming contribution to shear momentum appears to be smaller in the homogeneous results. The homogeneous shear method could be analyzed exactly at low density (using the Boltzmann equation), but that calculation has not yet been carried out.
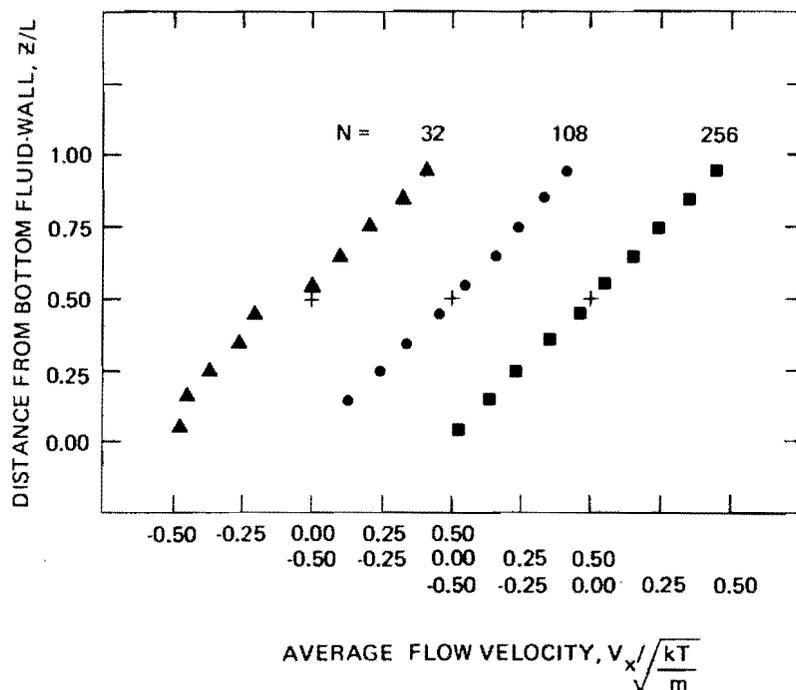
Fig. 11. Velocity profiles for systems undergoing plane Couette flow.
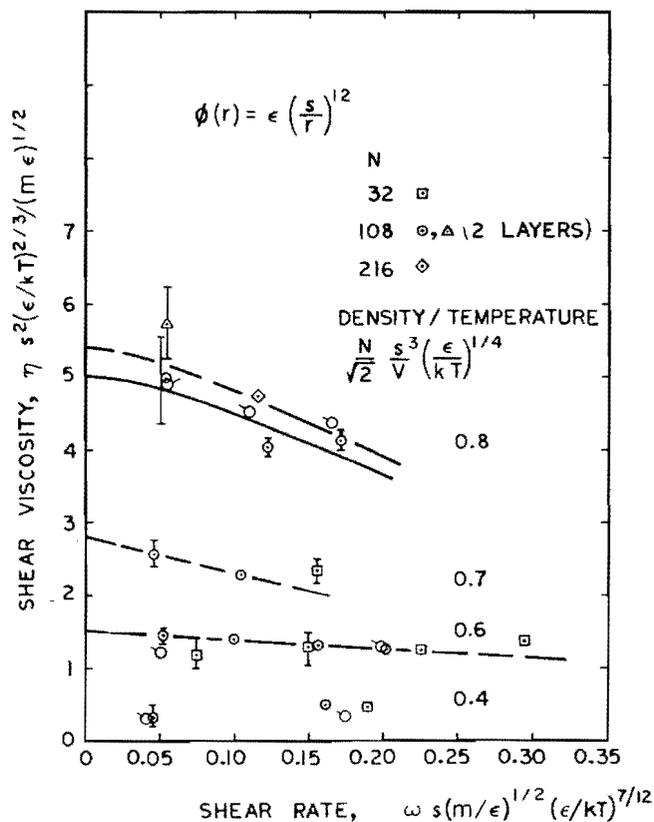
Fig. 12. Soft-sphere shear viscosity for several reduced densities as a function of shear rate. Results from homogeneous steady shear method are shown as flagged circles.

Table II

Soft-Sphere Shear Viscosity from Nonequilibrium Molecular Dynamics. Dependence on System Size, Density (for the Isotherm $\varepsilon = kT$), and Shear Rate[a]

N	$\dfrac{Ns^3}{\sqrt{2}\,V}$	$\omega s\left(\dfrac{m}{\varepsilon}\right)^{1/2}$	$\dfrac{\eta s^2}{(m\varepsilon)^{1/2}}$	Time
32	0.4	0.19	0.45 ± 0.03	64
108	0.4	0.16	0.50 ± 0.01	48
		0.05	0.33 ± 0.1	12
32	0.6	0.29	1.37 ± 0.08	64
		0.22	1.26 ± 0.08	48
		0.15	1.30 ± 0.17	48
		0.08	1.18 ± 0.22	16
108	0.6	0.21	1.25 ± 0.04	48
		0.16	1.30 ± 0.02	48
		0.10	1.38 ± 0.04	24
		0.05	1.44 ± 0.1	16
32	0.7	0.16	2.34 ± 0.17	48
108	0.7	0.11	2.27 ± 0.06	32
		0.05	2.54 ± 0.2	16
108	0.8	0.17	4.14 ± 0.12	48
		0.12	4.05 ± 0.13	32
		0.05	4.96 ± 0.6	16
		0.05^+	5.7 ± 0.5	16
216	0.8	0.12	4.7 ± 0.1	64

[a] N (= 32 and 108) soft spheres in a cube with N_w (= 8 and 18) particles in each boundary region (+ indicates $N_w = 36$). The 216 system is two 108-particle cubes wide. The shear rate is determined from average flow velocity in ten zones of bulk fluid. Apparent shear viscosity from average wall shear stress and shear rate. The dilute gas value is 0.17. The total observation time is given in terms of relative displacement of the boundary regions (in units of the cube edge $V^{1/3}$).

For liquid argon, the above conditions correspond to gigantic shear rates, of order 10^{10}/sec. However, a similar shear rate dependence has been experimentally observed at small shear rates for materials composed of long complicated molecules (e.g., grease, shaving cream, and fruit jam) (Sisko, 1958).

The direction of nonlinear effects depends upon the particular flowfield being studied. Shear viscosity is sometimes determined from the drag force

on a sphere moving through a fluid. For slow motion of a σ diameter sphere, the drag force is

$$\mathbf{F} = -3\pi\eta_0\sigma\mathbf{v}(1 + \tfrac{3}{16}\,\mathrm{Re} + \cdots) \tag{15}$$

where the first term is Stokes' linearized solution and the second term is due to Oseen who approximated the effect of the inertia terms. If the linear drag–velocity relation is used to define an effective viscosity, then an *increase* with sphere velocity is found; see Fig. 13. The abrupt decrease in drag (due to a turbulence-induced-wake-flow-pattern change) would limit a velocity expansion for the effective viscosity.
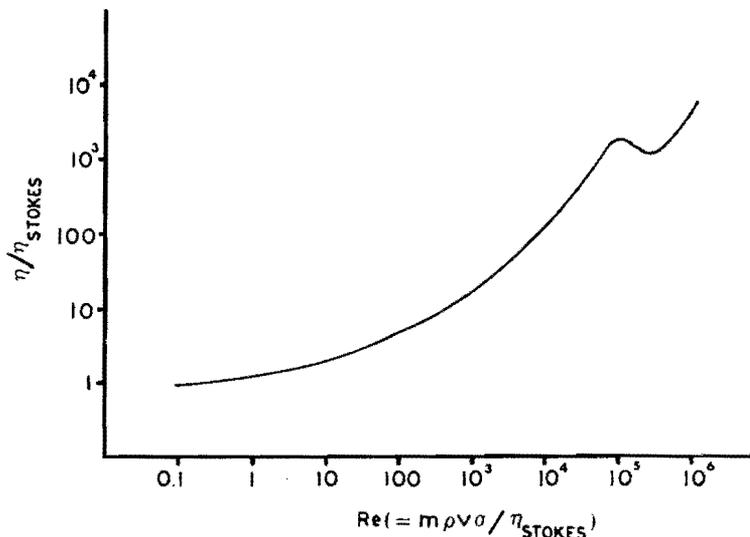
Fig. 13. Variation of the viscous drag on a sphere with Reynolds number. If the force is used to define an effective viscosity $\eta \equiv -F/(3\pi\sigma v)$, the ratio of η to the low-velocity value η_s varies by three orders of magnitude.

Because no quantitative theory for the dependence of viscosity on shear rate exists, apart from the low-density limit series expansion, we have chosen to use the semiempirical Ree–Eyring relation (Ree *et al.*, 1958)

$$\eta = \eta_0\,\sinh^{-1}(\omega\tau)/(\omega\tau), \tag{16}$$

which expresses the shear viscosity as a function of the zero-gradient hydrodynamic viscosity η_0, the shear rate ω, and the relaxation time τ. It is interesting to note that a fit of the soft-sphere data at a reduced density of 0.8 leads to a relaxation time of $9.2s(m/\varepsilon)^{1/2}(\varepsilon/kT)^{7/12}$, so that most of the molecular dynamic data lie beyond the radius of convergence of the series expansion of Eq. (16):

$$\eta = \eta_0[1 - (\omega\tau)^2/6 + 3(\omega\tau)^4/40 - \cdots] \qquad \text{for} \quad |\omega\tau| < 1. \tag{17}$$

Thus, even if it could be achieved, a theoretical prediction of the expansion coefficients in Eq. (17) would not be useful in reproducing the molecular-dynamic results at shear rates greater than $1/\tau$. The data could be fitted nearly as well with a linear gradient dependence, but we have rejected that approach since it leads to a vanishing viscosity at finite strain rates.

The computer results for the zero-shear-rate shear viscosity at $x = 0.4$, 0.6, 0.7, and 0.8 can all be summarized by the empirical relation

$$\eta s^2(\varepsilon/kT)^{2/3}/(m\varepsilon)^{1/2} = 0.149 + 0.022 \exp(6.83x), \qquad (18)$$

where x is the reduced density/temperature $(Ns^3/\sqrt{2}\,V)(\varepsilon/kT)^{1/4}$. This relation, required to have the zero density value of 0.171, produces a first density correction $(x \to 0)$ that is only 10% larger than the Enskog estimate. Shear viscosity predictions from the paradigms of Andrade and Enskog are compared with the computer results in Fig. 14.
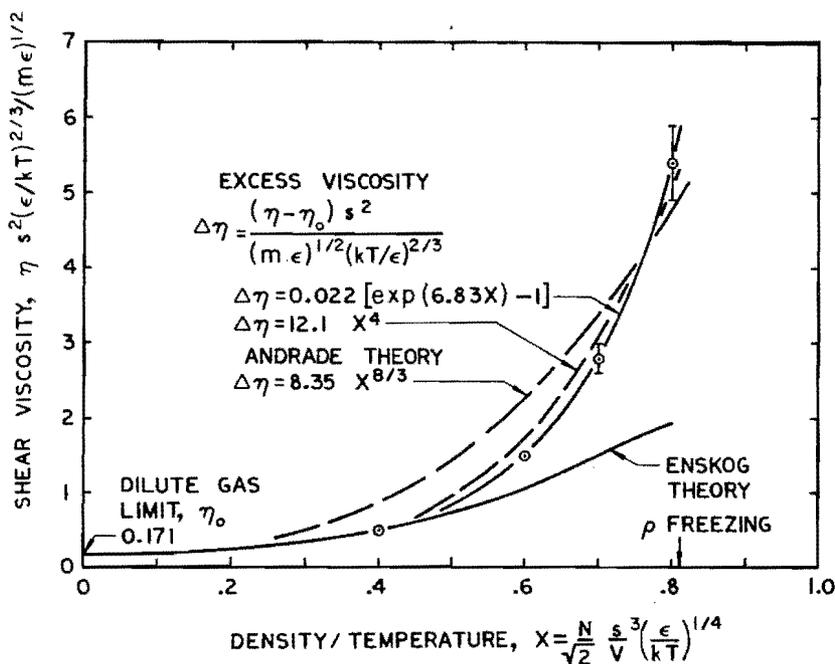
Fig. 14. Soft-sphere shear viscosity. The machine results are compared with two empirical power-law fits and with the predictions of two approximate theories of shear viscosity, Enskog's and Andrade's. Estimated zero shear rate viscosity from $N = 108$ results.

Andrade (1934) suggested that a fluid-phase particle undergoing viscous flow oscillates about its temporary location, transferring transverse momentum to its neighbors at its turning points. For soft spheres, this idea leads to the relation

$$\eta s^2(\varepsilon/kT)^{2/3}/(m\varepsilon)^{1/2} = 8.35x^{8/3}. \qquad (19)$$

Figure 14 indicates that Andrade's model is an excellent approximation to the computed shear viscosity, but somewhat underestimates the density dependence. Shown also in Fig. 14 are the predictions of Enskog's approximate model, which predicts viscosities too low by approximately a factor of two near the freezing density. The Enskog model, based on a hard-sphere diameter calculated from the equation of state, was found by Alder *et al.* (1970) to give similar deviations from computer measured hard-sphere shear viscosities.

Although the soft-sphere results suggest that the nonequilibrium molecular dynamic method does produce reliable transport coefficients, the accuracy of the method is not likely to be better than 5% with present computers.

An approximate model for the *structure* of a sheared fluid can be developed under the assumption that shear strain relaxes with a typical relaxation time τ'. Thus a fluid undergoing shear at shear-rate ω would have the same structure as that obtained by elastic distortion of the fluid with strain angle $\omega\tau'$. This simple model, based on ideas due to Maxwell, predicts that the nonequilibrium part of the pair distribution function, which contributes the shear stress P_{xy}, is proportional to $r \, dg/dr$ where g is the equilibrium pair distribution function. Figure 15 indicates that this relation is approximately valid. The relaxation time τ' found, however, is somewhat different from that of the Ree–Eyring theory τ. For example, at a reduced density of 0.8, Maxwell's relaxation time, $\tau' = 0.11 \, s(m/\varepsilon)^{1/2}(\varepsilon/kT)^{7/12}$ corresponds to about one-fourth the oscillator period, $0.45s(m/\varepsilon)^{1/2}(\varepsilon/kT)^{1/2}$, in accord with Andrade's model. The Ree–Eyring time τ is much longer, by two orders of magnitude, and corresponds to the time required for a particle to *diffuse* the distance separating nearest neighbors. Thus the different relaxation times show that the *mechanism* for viscous flow *does* involve interparticle vibrations but the *rate-dependence* of that mechanism involves the relaxation of shear stress through the diffusion of particles.

2. Lennard-Jones Potential

If a sixth-power attraction is added to the twelfth-power soft-sphere repulsion, the Lennard-Jones potential results:

$$\phi = 4\varepsilon[(\sigma/r)^{12} - (\sigma/r)^{6}]. \tag{20}$$

The coefficient 4 provides a minimum potential value of $-\varepsilon$, where $(\sigma/r)^6 = \frac{1}{2}$. The Lennard-Jones potential produces both kinds of fluid phases: gas and liquid. The phase diagram, determined by equilibrium molecular dynamics and Monte Carlo calculations (Hansen and Verlet, 1969), is shown in Fig. 16. The phase diagram for argon corresponds closely with the computer generated one if the characteristic energy ε and length σ are chosen to be 119.8°K and 3.405 Å respectively. This correspondence
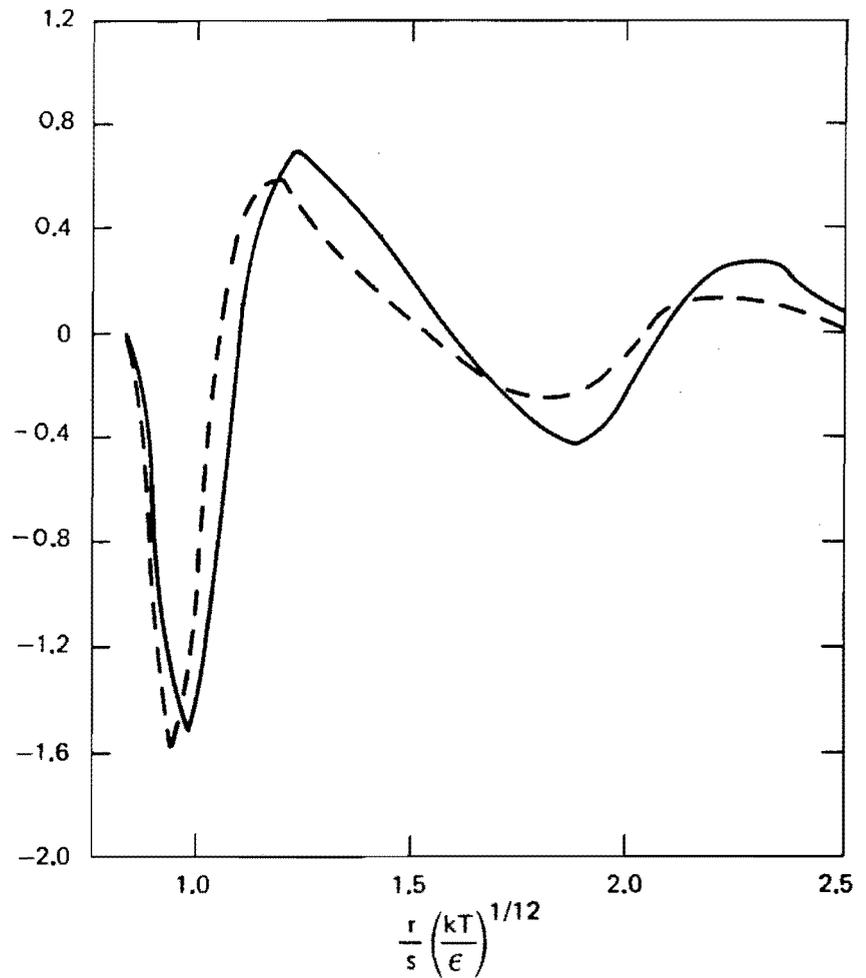
Fig. 15. Comparison of the measured nonequilibrium pair distribution function (solid line) with the predictions of the approximate relaxation-time theory (dash line). The relaxation time τ' is a parameter chosen so that the approximate distribution function will produce the measured shear viscosity.
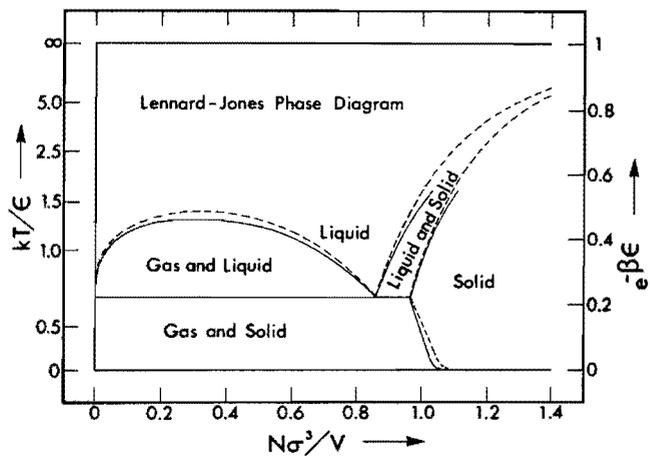
Fig. 16. Comparison of the Lennard-Jones phase diagram with the phase diagram for argon. The dashed phase lines were determined in computer experiments using the Lennard-Jones potential. The heavy lines correspond to phase lines for argon.

suggests a comparison of calculated transport coefficients for the Lennard-Jones potential with experimentally determined transport coefficients for argon.

Along the saturated vapor pressure line the shear viscosity of liquid argon has been characterized by three different methods (Boon *et al.*, 1967; DeBock *et al.*, 1967; Hellemans *et al.*, 1970; Haynes, 1973). The results are compared with nonequilibrium molecular dynamics results in Fig. 17. The molecular dynamics values have been extrapolated to zero shear rate, using the Ree–Eyring theory; see Table III. The agreement with the experimental data is good, again indicating that the Lennard-Jones potential is a useful representation for liquid argon.

Near the triple point, the computer results depend strongly upon both the number of particles used and the shear rate ω. Thirteen separate calculations, for systems of 108, 216, and 324 particles sandwiched between boundary regions containing 18 particles each, were carried out, and are summarized in Table IV. The results clearly depend upon system width.
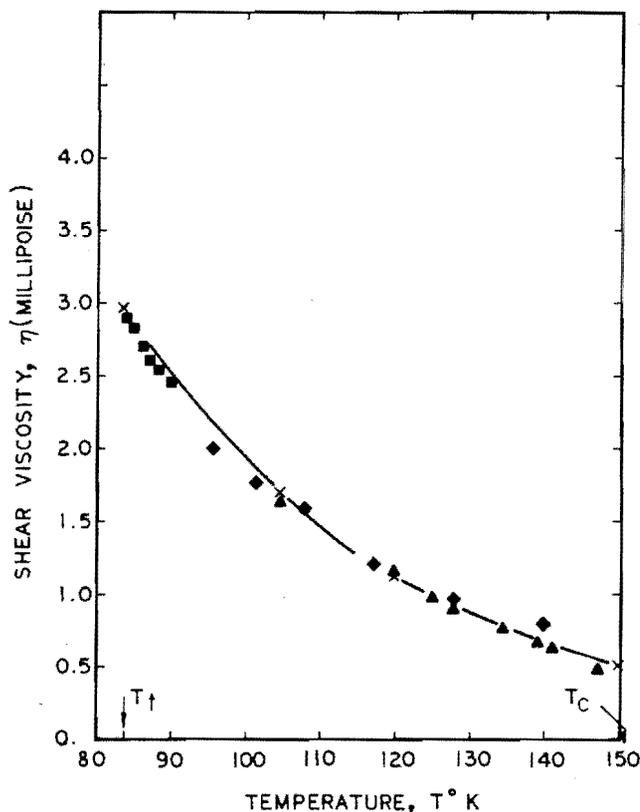
Fig. 17. Comparison of the Lennard-Jones shear viscosity with the shear viscosity for argon along the saturated vapor pressure line. ($\times$) Lennard-Jones via nonequilibrium molecular dynamics ($\sigma = 3.405$ Å, $\varepsilon/k = 119.8°$K). Experiment: (■) Boon, (◆) De Bock, (▲) Hellemans.

Table III

SHEAR VISCOSITIES FROM NONEQUILIBRIUM MOLECULAR DYNAMICS ALONG THE SATURATED
VAPOR PRESSURE LINE FOR ARGON[a]

				$\eta\sigma^2/(m\varepsilon)^{1/2}$		
$N\sigma^3/V$	kT_0/ε	kT/ε	$\omega\sigma(m/\varepsilon)^{1/2}$	Calculated	Estimated for $\omega = 0$	Enskog estimate
0.4774	1.228	1.192	0.116	0.55_4		
		1.220	0.079	0.59_3	0.64	0.53
0.6920	0.998	0.982	0.135	1.1_8		
		0.972	0.086	1.3_0	1.39	1.19
0.7608	0.872	0.840	0.123	1.8_4		
		0.860	0.083	1.8_2	1.92	1.70
0.8531	0.701	0.684	0.112	3.5_1		
		0.700	0.075	3.9_6	4.21^b	2.87

[a] All of the results shown are for 108 particles with two boundary regions containing 18 particles each. T_0 is the boundary temperature and T is the temperature measured in the bulk fluid over a time period of $64V^{1/3}(m/kT_0)^{1/2}$. The zero-shear-rate estimates are based on (1) an inverse hyperbolic sine dependence of viscosity on strain rate; and, (2) for the two lower temperatures, a constant-volume temperature dependence of $(\partial \ln \eta/\partial \ln T)_v = -0.65$. Also shown are the predictions of the Enskog model using the computer-generated equation of state for the Lennard-Jones potential.
[b] The width dependence of the triple-point shear viscosity suggested by the data of Table IV is $\eta_{\kappa'}/\eta_{0,0} = 1 + 1.4\kappa'$, where κ' is the ratio of σ to the system width in the gradient direction. Applying this correction to the 108 particle triple-point viscosity yields the estimate $\eta_{0,0} = 3.29(m\varepsilon)^{1/2}/\sigma^2$.

There are two reasons for expecting an inverse-width correction:

(i) such a correction correlates experimental results for spheres dropping down tubes of finite width (Partington, 1955);

(ii) such a correction correlated single-particle displacement moduli in harmonic crystals; there is a mathematical correspondence between the moduli of such crystals and the viscosity for fluids (Hoover et al., 1974).

A least-squares fit of all of the triple-point data to the form

$$\eta_{\omega, \kappa'} = \eta_{0,0}(1 + c\kappa') \sinh^{-1}(\omega\tau)/(\omega\tau) \qquad (21)$$

yields the values of $2.95(m\varepsilon)^{1/2}/\sigma^2$ for $\eta_{0,0}$, 1.376 for c—the width correction, and $8.7\sigma(m/\varepsilon)^{1/2}$ for τ. Figure 18 illustrates the correlation obtained using this three-parameter fit. The extrapolated hydrodynamic viscosity $\eta_{0,0}$ agrees, within 2%, with the experimental triple-point viscosity for argon. The homogeneous shear method (external forces are used *throughout* the

Table IV

SHEAR VISCOSITIES FROM NONEQUILIBRIUM MOLECULAR DYNAMICS NEAR THE LENNARD-JONES TRIPLE POINT. DEPENDENCE ON SYSTEM WIDTH (ONE, TWO, AND THREE 108-PARTICLE CUBES WIDE) AND SHEAR RATE[a]

			$\eta\sigma^2/(m\varepsilon)^{1/2}$	
N	$\omega\sigma(m/\varepsilon)^{1/2}$	kT/ε	Calculated	Adjusted
108	0.248	0.672	2.85 ± 0.06	2.72
	0.156	0.699	3.07 ± 0.06	3.01
	0.113	0.711	3.28 ± 0.06	3.24
	0.0852^+	0.713	3.41 ± 0.09	3.38
	0.0737	0.715	3.54 ± 0.11	3.52
	0.0371	0.724	3.72 ± 0.22	3.72
216	0.112	0.681	3.08 ± 0.05	2.96
	0.0885^+	0.699	3.21 ± 0.09	3.14
	0.0825	0.689	3.25 ± 0.15	3.15
	0.0399	0.721	3.38 ± 0.17	3.37
324	0.0872	0.670	3.04 ± 0.05	2.90
	0.0416	0.707	3.16 ± 0.06	3.12
	0.0200	0.717	3.23 ± 0.17	3.22

[a] There are 18 particles in each boundary region (+ indicates 36). In each case $N\sigma^3/V$ is 0.8442 and the boundary temperature is $T_0 = 0.722\varepsilon/k$. The observation time is 96, 64, and $80L(m/kT_0)^{1/2}$, where L is the 108-particle cube edge. Both the measured viscosity and the adjusted value [estimated constant volume temperature dependence is $(\partial \ln \eta/\partial \ln T)_v = -0.65$] are shown as is the average bulk fluid temperature.

system to maintain the shear flow; see Fig. 9) has also been used for the triple point. The dashed line in Fig. 18 represents the results of 108- and 216-particle systems which indicate *no* width dependence with a smaller relaxation time $[5.5\sigma(m/\varepsilon)^{1/2}]$. The extrapolated zero-shear-rate viscosity agrees with the nonequilibrium shear flow result and with the experimental argon value.

Although the corrections which have been applied to the nonequilibrium results are a bit arbitrary, an overall picture has emerged which is self-consistent and also consistent with experimental shear viscosities. The one puzzling point which remains is the disagreement with the viscosity determined from the Green–Kubo relations by Verlet's group (Levesque *et al.*, 1973). The Green–Kubo triple-point value for 864 Lennard-Jones particles with periodic boundaries exceeds our hydrodynamic estimated viscos-
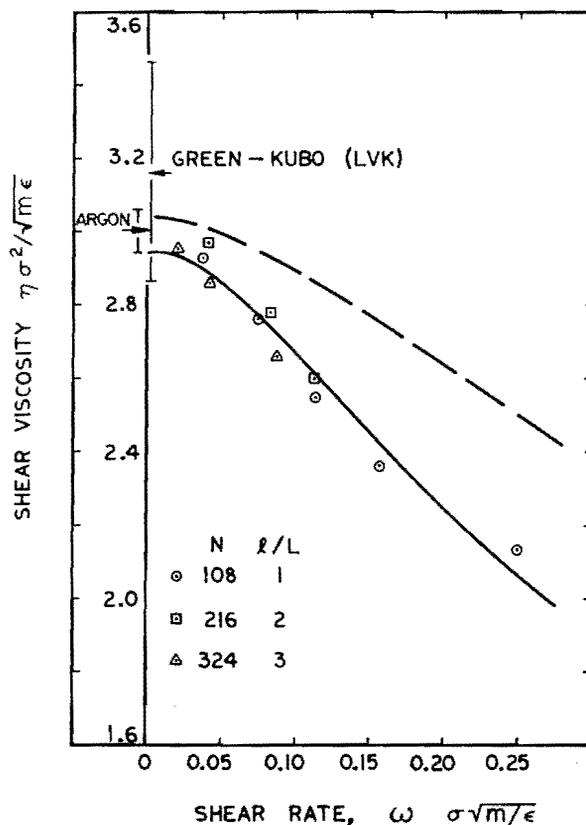
Fig. 18. Shear viscosity for various systems and shear rates using the Lennard-Jones potential under conditions corresponding to the triple point. In addition to the results from plane Couette flow, the results determined from homogeneous steady shear (dashed curve) are also shown. The large-system results for both methods should agree at low shear rates. The width-adjusted Green-Kubo result is also shown.

ity by about 30%. The two kinds of calculations could be brought into agreement *if* the number-dependence of the Green–Kubo results at the triple point varied as $1 + 2c\kappa'$, that is with twice the width correction of the direct molecular dynamic method. Only a more detailed investigation of smaller systems with the Green–Kubo method can establish the Green–Kubo number dependence.

Additional detailed studies of the Lennard-Jones viscosity along the freezing line and at two relatively high temperatures, $kT/\varepsilon = 8.5$ and 28 were carried out. Figure 19 shows that the calculated excess shear viscosity $\Delta\eta$ [$\equiv \eta - \eta_0$, where η_0 is the dilute gas value], when expressed in the soft-sphere scaling variables, has the functional form of x^4 or $e^{bx} - 1$, where x is $(N\sigma^3/V)(\varepsilon/kT)^{1/4}$.

These functional forms reveal two features: (1) weak temperature dependence, and (2) a negative isochoric temperature derivative. While both of these features have been experimentally observed in simple fluid shear-
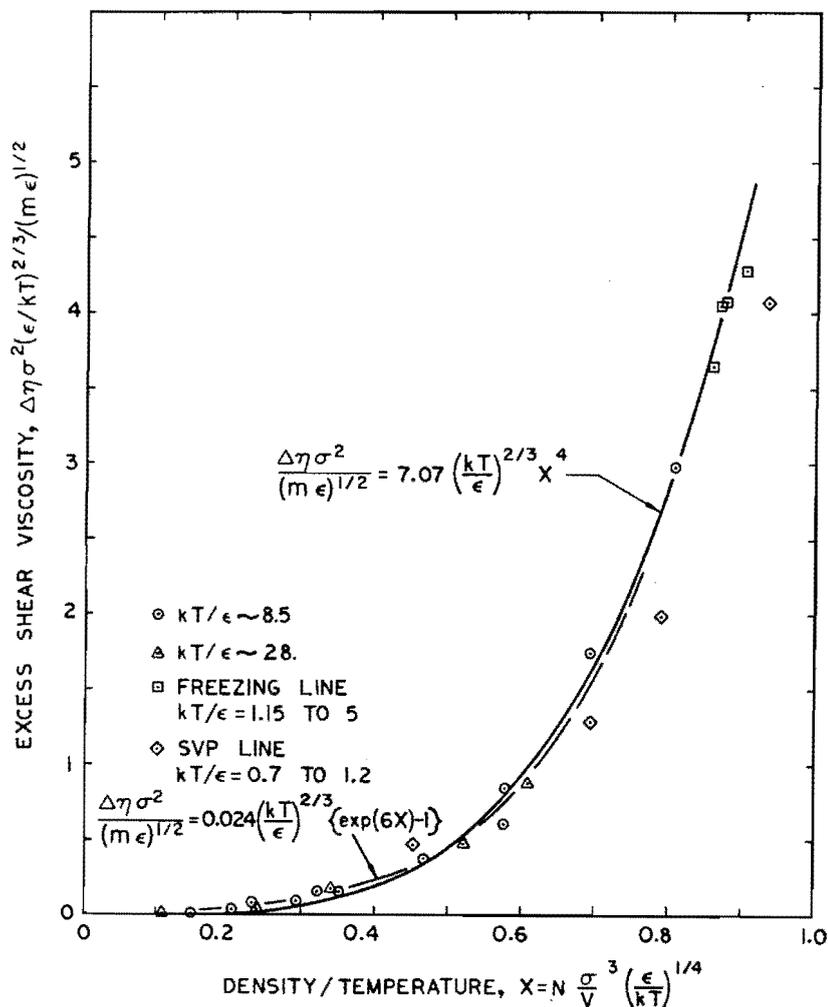
Fig. 19. Lennard-Jones excess shear viscosity from plane Couette flow as a function of the soft-sphere variable x which combines the density and temperature scales.

viscosity data [e.g., argon, helium, hydrogen, oxygen, and carbon dioxide; see Hanley *et al.* (1972)], their cause has not been previously traced to the dominance of the repulsive core potential.

All of the results obtained from nonequilibrium molecular dynamics can be summarized by the empirical relation (chosen to reduce to the soft-sphere form at high temperatures)

$$\Delta\eta\sigma^2(m\varepsilon)^{-1/2}(\varepsilon/kT)^{2/3} = 0.0152[1 - \tfrac{1}{2}(\varepsilon/kT)^{1/2} + 2(\varepsilon/kT)]$$
$$\times \{\exp[7.02x(1 - \tfrac{1}{5}(\varepsilon/kT)^{1/2})] - 1\}. \quad (22)$$

The usefulness of the reduced variable x in fitting Lennard-Jones viscosity data suggests the use of a similar fit for experimental data for argon (Michels *et al.*, 1953; Haynes, 1973). The data range from reduced temperatures kT/ε

of 0.7 to 2.9 and from dilute gas to saturated liquid densities. All of these data can be expressed economically by the form

$$\Delta\eta\sigma^2(m\varepsilon)^{-1/2}(\varepsilon/kT)^{2/3} = 0.0324[\exp(5.18x) - 1]. \qquad (23)$$

The Lennard-Jones calculations just described indicate that viscosities can be measured via nonequilibrium molecular dynamics throughout most of the fluid portions of the phase diagrams. The accuracy is not equal to that with which equilibrium thermodynamic properties are measured. At the same time the results do appear to be just as accurate as those derived from the Green–Kubo method and have the added advantages of displaying directly nonlinear and structural transport information. The correlation between the soft-sphere and Lennard-Jones viscosities suggests, in accord with Enskog's model, that real fluid properties be expressed in terms of the scaled variables appropriate for repulsive forces.

3. Two-Dimensional Systems

There is certainly no prospect for finding real two-dimensional systems in our three-dimensional world. Nevertheless the transport coefficients are particularly interesting in two dimensions. This is because theoretical predictions (Keyes and Oppenheim, 1973; Wood, 1973) suggest that the coefficients "diverge," without providing a physical interpretation of the divergence. Because it is physically obvious that any finite system undergoing shear at a finite rate must have a finite shear stress, the divergence can only be understood as a limiting process as the size of the system increases and the gradient decreases. The theoretical predictions for *finite* systems undergoing steady transport have not yet been worked out.

To assess the significance of the theoretical predictions, a study of two-dimensional "soft-disk" systems was carried out (Hoover *et al.*, 1974). The density chosen was about half the freezing density. The interparticle potential was

$$\phi(r) = \varepsilon(s/r)^{12} \qquad (24)$$

Figure 20 is from a computer generated movie for 98 soft disks and presents both the long-time average and instantaneous velocity profile. The movie clearly reveals the increase of collisions in the $x = y$ direction relative to the $x = -y$ direction. These collisions generate the potential part of P_{xy}. The flow pattern does not appear anomalous. The results of nine separate calculations for $N = 32, 50, 98,$ and 392 are shown in Table V. It is interesting to see that, within the relatively large 10% statistical uncertainty, there is no clear-cut dependence of the two-dimensional viscosity on either system size or shear rate.

If we apply the two approximate models for fluid viscosity, Andrade's and
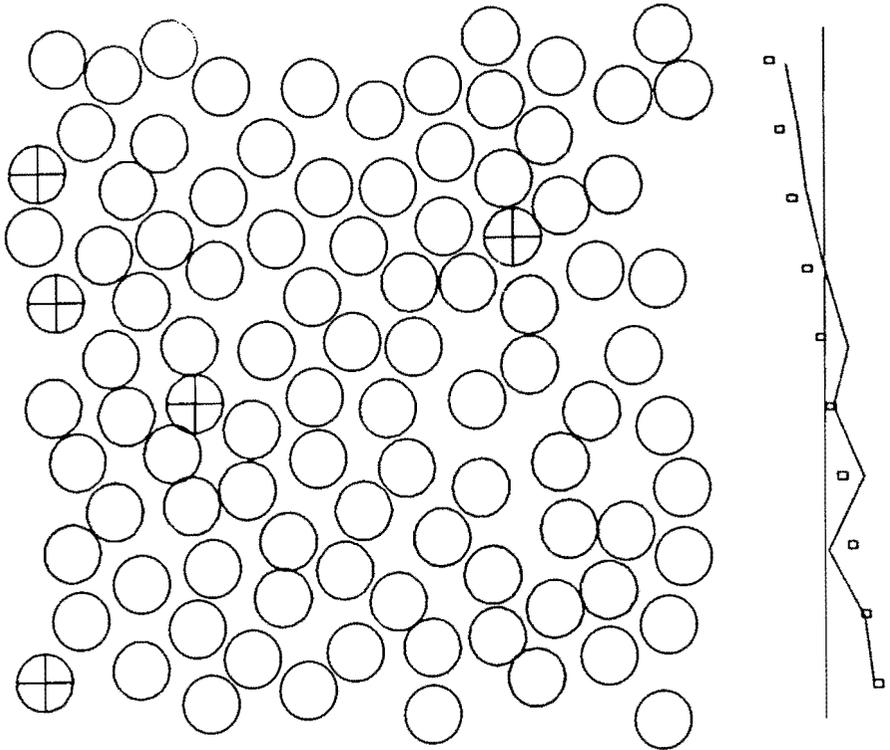
Fig. 20. Typical movie frame showing 98 soft disks undergoing plane Couette flow. The particles are driven by two boundary regions, of 14 particles each, maintained at constant speed. The viscosity is determined from the shear stress and the velocity gradient $\eta \equiv -P_{xy}/\omega$. The instantaneous velocity profile (solid line) and its long-time average (squares) are also shown.

Enskog's, to this two-dimensional situation both predictions turn out to be consistent with the nonequilibrium molecular dynamic results, $\eta = (m\varepsilon)^{1/2}/s$, within about 10%.

What are we to make of these patently nondivergent results? First, we can conclude that the hydrodynamic behavior of small two-dimensional dense-fluid systems *can* be usefully described by the linear transport laws applicable to three-dimensional systems. In order to reconcile our results with the predictions of divergence, the latter phenomenon must lie well outside the region in which viscosity is a useful concept. When we try to study the region in relative wall velocity–coordinate space in which it is meaningful to characterize the pressure tensor with shear viscosity, we find somewhat different results from those characterizing three-dimensional systems.

Just as in three dimensions, consider a volume element at a temperature T with sidelength L and velocity gradient $\omega = v/L$. First, the volume element should be more than a few diameters wide, $L/s > 3$. Second, the Reynolds number for the volume element should be small enough to suppress macroscopic turbulence, Re < 1500, so that the flow will be laminar and

Table V

SOFT-DISK SHEAR VISCOSITIES FROM NONEQUILIBRIUM MOLECU-
LAR DYNAMICS AT REDUCED DENSITY, $Ns^2(\frac{3}{4})^{1/2}/V$ OF 0.6[a]

N	$\omega s(m/\varepsilon)^{1/2}$	kT/ε	$\eta s/(m\varepsilon)^{1/2}$	Time
32 + 8	0.072	1.06	1.00 ± 0.10	6
32 + 16	0.075	1.00	1.23 ± 0.08	6
50 + 20	0.043	0.49	1.12 ± 0.08	8
50 + 20	0.033	1.00	0.92 ± 0.21	2
50 + 20	0.056	0.98	1.22 ± 0.09	4
50 + 20	0.074	1.47	1.05 ± 0.11	8
98 + 28	0.041	0.99	1.14 ± 0.09	5
98 + 28	0.181	0.71	0.94 ± 0.02	9
392 + 56	0.042	0.94	1.02 ± 0.05	1

[a] The notation $N = 32 + 8$ indicates 32 particles in the unit
square with four particles in each of the two boundary regions.
The observation time is given in terms of relative displacement
of the boundary regions (in units of the square edge).

steady $(L/s)v(m/\varepsilon)^{1/2} < 2165$. Third, the dissipation of the shear stress
(energy/time = ηv^2), ought to produce less than a 10% temperature differ-
ence between the center and the boundary of the region being studied.
Hydrodynamics indicates that the temperature difference is $\eta v^2/8\kappa$. We use
the estimate $5(k/s)(\varepsilon/m)^{1/2}$ for the conductivity, giving $mv^2 < 4kT$. Last, the
shear stress due to the viscosity ought to be reasonably large, say at least
10% of the natural fluctuations in the volume element. As an estimate of the
pressure fluctuations we use $N^{1/2}kT/L^2$ so that $\eta v/L > 0.08kT/(Ls)$.

Each of the four conditions bounding the region of useful two-
dimensional viscosity corresponds to a restriction on the two dimensionless
variables L/s and $v(m/\varepsilon)^{1/2}$. These conditions, plotted in Fig. 21, differ from
the three-dimensional conditions appearing in Fig. 10. Notice particularly
that the last two conditions are independent of the volume element's size L.
This means that in order for the shear stress to be observably large, v cannot
be made arbitrarily small. Thus the usual limiting case in three dimensions,
$v \rightarrow 0$, does not apply in two dimensions. It seems likely that the source of
the two-dimensional divergences is simply the greater significance of fluctua-
tions in two-dimensional systems, where low-frequency disturbances play an
enhanced role. These disturbances are presumably responsible for the rela-
tively low 10% accuracy of the two-dimensional results.

A related divergence is associated with two-dimensional *crystals*, in which
the thermodynamic rms displacement of a particle from its lattice site is
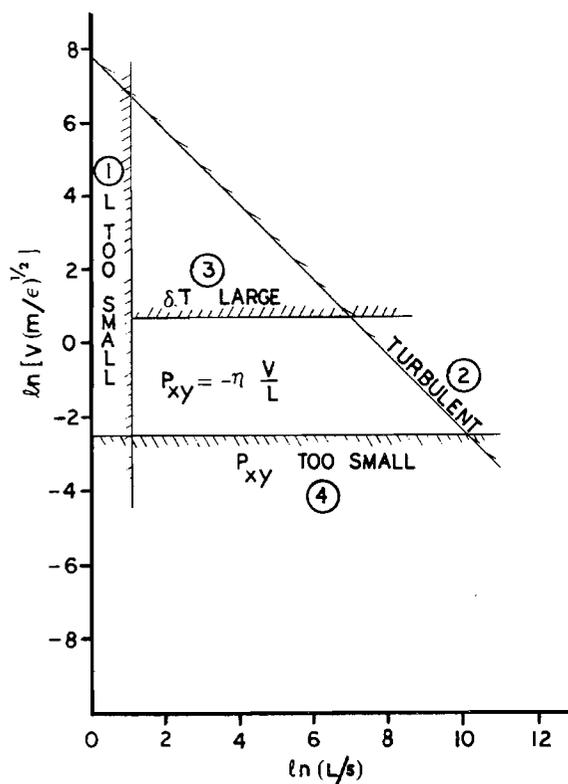
Fig. 21. Limitations on the sidelength L and the relative velocity V for a square of soft disks at a reduced density of 0.6 and a temperature $\varepsilon = kT$. As in Fig. 10 the four lines correspond to the restrictions of (1) size, (2) laminar flow, (3) small temperature gradients, and (4) observable shear stress. Macroscopic hydrodynamics is useful for describing flows within the central quadrilateral.

divergent. The divergence occurs very slowly, however, as N is increased, varying with N as the square root of $\ln N$. In a two-dimensional crystal spanning the known universe (10^{10} ly across) the rms displacement at the melting point would still be less than 10 Å (Hoover *et al.*, 1974).

We can anticipate further investigations of two-dimensional systems which offer a variety of interesting divergences absent in three dimensions.

C. THERMAL CONDUCTIVITY

Thermal conduction can also be simulated with nonequilibrium molecular dynamics. To do so we maintain the two boundary regions surrounding the bulk fluid at different temperatures rather than different velocities. Because the conductivity is measured at mechanical equilibrium it is appropriate that the two boundary regions have slightly different densities, chosen so that the pressure, as a function of the boundary density and temperature, is the same for both regions. Temperature, density, and compressibility factor profiles are shown in Fig. 22 for 108 soft spheres at three-fourths the
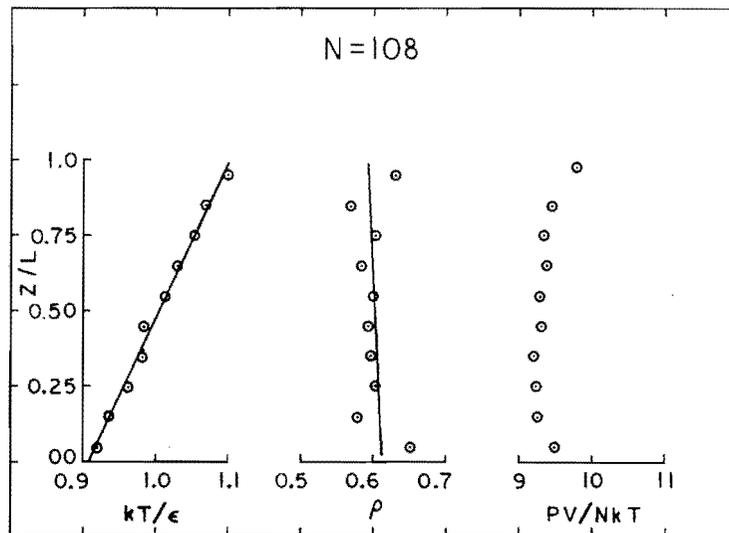
Fig. 22. Profiles of temperature, density, and compressibility factor in a soft-sphere system undergoing heat flow at about three-fourths the freezing density.
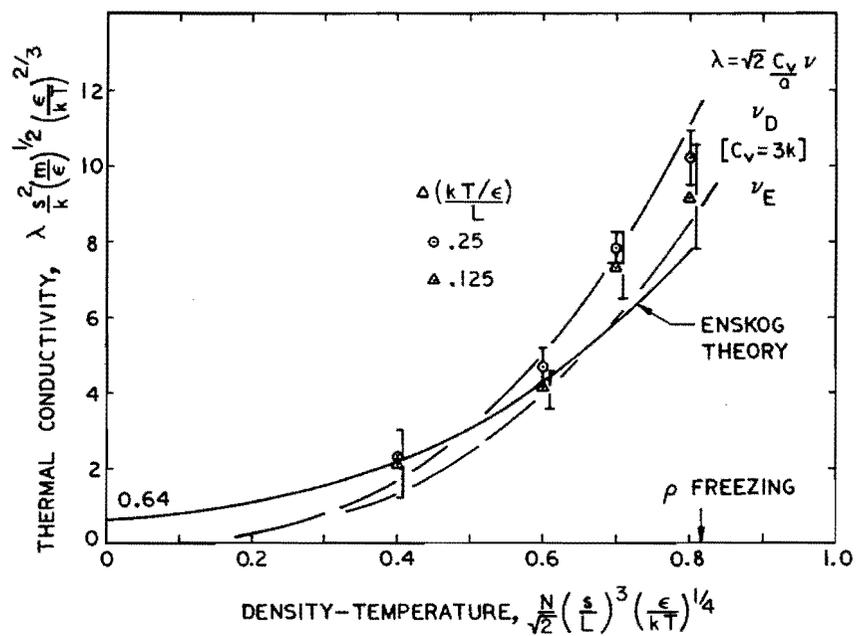
Fig. 23. Thermal conductivity for 108 soft spheres at several fluid-phase densities. The three curves correspond to approximate theories of thermal conductivity, Enskog's, and a theory based on a vibrational transfer model. The two vibrational-model curves correspond to different choices for the vibrational frequency, Debye's v_D and Einstein's v_E.

freezing density. The soft-sphere calculations, shown in Fig. 23, provide thermal conductivities with uncertainties of order 10% throughout the dense-fluid portion of the phase diagram. These results suggest a nonlinear thermal conductivity dependence which increases with temperature gradient. We know of no experimental evidence for (or opposed to) this effect. The gradients involved are quite large, of order 100 keV/cm!

The soft-sphere results for thermal conductivity differ from shear viscosity in that the conductivity is in reasonable agreement with the Enskog estimate over the complete fluid density range (compare Figs. 23 and 14). Smaller deviations compared to shear viscosity were also found for the hard-sphere thermal conductivity by Alder *et al.* (1970). McLaughlin and Horrocks (1964) suggested an oscillator model for energy transport that is physically identical to Andrade's viscosity model. For the dense fluid state, an oscillating particle exchanges energy (rather than momentum) with its neighbors at each turning point. Just as in the case of viscosity, the oscillator model provides a better description of dense-fluid transport than does the Enskog model (Fig. 23).

An extensive series of thermal conductivity calculations was carried out for the Lennard-Jones potential. The effect of the attractive potential was to increase somewhat the uncertainty in the conductivity, particularly at low temperature, and also, at high density, to change the sign of the nonlinear
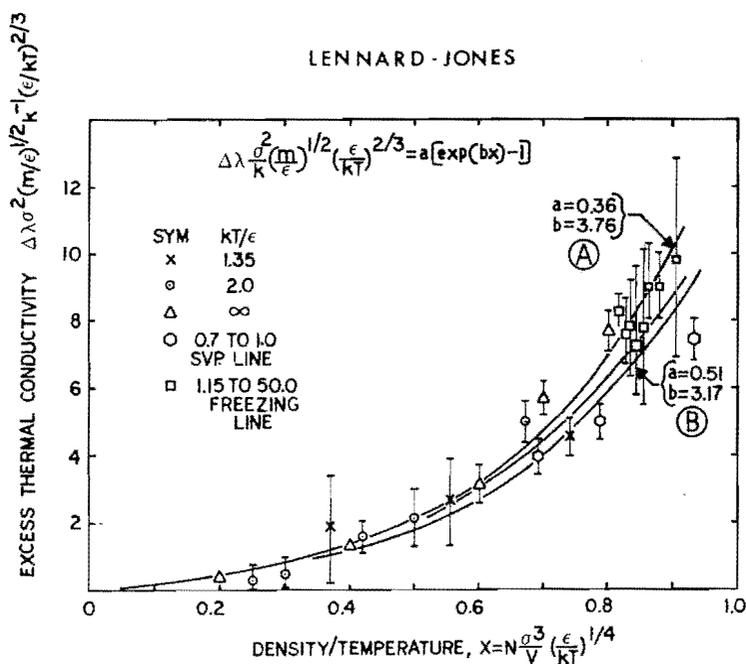
Fig. 24. Thermal conductivity for the Lennard-Jones potential as a function of the soft-sphere variable x which combines the density and temperature scales. The vertical lines denote $\pm$ one standard deviation.

dependence of conductivity on temperature gradient. Because the Lennard-Jones excess shear viscosity could be correlated with the soft-sphere scaling variables, a similar scaling of the excess thermal conductivity results was carried out, as shown in Fig. 24. The difference in thermal conductivity from the low-density value can be expressed economically by the relation

$$\Delta\lambda(\sigma^2/k)(m/\varepsilon)^{1/2}(\varepsilon/kT)^{2/3} = a[\exp(bx) - 1], \tag{25}$$

where the constants a and b depend somewhat upon the data temperature range. Fitting of experimental argon data yields similar coefficients, which for densities less than twice critical, provide a *positive* ischoric temperature derivative (the opposite of shear viscosity). This same qualitative difference has been found experimentally for hydrogen, helium, and other simple fluids (Hanley *et al.*, 1972).

V. Prospects

What does the future hold for computer experiments with nonequilibrium systems and how will the theoretical interpretation of such experiments develop? It has already been demonstrated that computers can provide transport coefficients accurate within about 5–10% for simple monatomic systems. Because the efficiency of the calculations varies from method to method, it seems likely that greater accuracy will be obtained with more ingenious approaches to the nonequilibrium problems. Nevertheless the calculations are time-consuming, involving either the decay of equilibrium fluctuations or the establishing of a nonequilibrium steady flux. In the future such calculations should be restricted to a few carefully studied and widely spaced points. Between these points approximate models such as Andrade's and Enskog's can be used as interpolation guides.

Ingenuity need not be limited to developing new schemes for measuring the transport coefficients themselves. The nonequilibrium computer experiments furnish the detailed approach to the nonequilibrium state and can be analyzed to obtain the nonequilibrium spatial and velocity distribution functions. These functions will certainly prove useful in building more detailed models of nonequilibrium structure. Because the computer experiments are limited to small lengths and times, the most potentially useful theoretical work is that which predicts the dependence of these small-system results on the chosen boundary conditions, size, and observation times. A thorough understanding of two-dimensional transport properties, supported by computer experiments, is an essential part of this program.

Computers naturally lend themselves to the study of transport with extremely large gradients—if the gradients are not large then the transport is

masked by fluctuations—as opposed to the more usual infinitesimal gradients of the Green–Kubo theory. The computer work should stimulate an experimental effort to identify higher order and nonlinear transport coefficients. The correlation of the nonlinear shear viscosity uncovered by the computer experiments with the phenomenological Ree–Eyring theory of large-molecule flow suggests that clever experiments could uncover a wide range of qualitatively new effects. From the theoretical viewpoint, the fact that most of the computer data lie beyond the radius of convergence of small-gradients series (if such series exist!) indicates that nonequilibrium series expansions are much less useful than the virial series expansions of equilibrium properties. Although there is no substitute for firmly grounded theory, it is clear that empirical models such as Eyring's and Andrade's are appropriate starting points for additional theoretical work.

The connection between the microscopic variables of molecular dynamics and the macroscopic variables of irreversible thermodynamics deserves critical study. For example, the many alternative ways of defining local pressure tensors ought to be systematically compared, in computer experiments, in order to devise recipes which provide the best atomistic analogy for continuum properties. Analysis of the response of systems to nonequilibrium boundary conditions should also make it possible to study the entropy and energy stored in nonequilibrium systems.

In addition to the microscopic interpretation of thermodynamics and hydrodynamics, there are many practical problems that can better be understood, for idealized models, through computer experiments. We expect to see many more such calculations in the next few years. To mention a few: dislocation motion, plastic flow, crack propagation, and shock propagation. Of these, the shock propagation problem is, in principle, the simplest because the boundary conditions are equilibrium ones.

In conclusion, today's computers make it possible to study a wide variety of problems of theoretical and practical interest. The combination of computer techniques with theoretical modeling that has proved so successful in providing our current understanding of equilibrium statistical thermodynamics should ultimately prevail in the much richer nonequilibrium field.

References

Aarseth, S. J. (1972). *In* "Gravitational *N*-Body Problem" (M. Lecar, ed.), p. 29. Reidel Publ., Dordrecht, Netherlands.

Alder, B. J. (1973). *Annu. Rev. Phys. Chem.* **24**, 325.

Alder, B. J., and Wainwright, T. E. (1958). *Proc. IUPAP Symp. Transport Processes Statist. Mech., 1956* p. 97.

Alder, B. J., and Wainwright, T. E. (1959). *J. Chem. Phys.* **31**, 459.

Alder, B. J., Gass, D. M., and Wainwright, T. E. (1970). *J. Chem. Phys.* **53**, 3813.

Andersen, H. C., Weeks, J. D., and Chandler, D. (1971). *Phys. Rev. A* **4**, 1597.

Andrade, E. N. Da C. (1934). *Phil. Mag.* [7] **17**, 497 and 698.

Ashurst, W. T. (1974). Ph.D. Dissertation, University of California at Davis-Livermore.

Ashurst, W. T., and Hoover, W. G. (1973). *Phys. Rev. Lett.* **31**, 206.

Barker, J. A., and Henderson, D. (1967). *J. Chem. Phys.* **47**, 2856 and 4714.

Barker, J. A., Bobetic, M. V., and Pompe, A. (1971). *Mol. Phys.* **20**, 347.

Beeler, J. R. (1966). *Phys. Rev.* **150**, 470.

Bird, G. A. (1970). *Phys. Fluids* **13**, 2676.

Boon, J. P., Legros, J. C., and Thomaes, G. (1967). *Physica (Utrecht)* **33**, 547.

Born, M., and Huang, K. (1954). "Dynamical Theory of Crystal Lattices." Clarendon Press, Oxford, England.

Chapman, S., and Cowling, T. G. (1960). "Mathematical Theory of Non-Uniform Gases." Cambridge Univ. Press, London and New York.

Contopoulos, G. (1966). "Theory of Orbits in the Solar System and in Stellar Systems." Academic Press, New York.

De Bock, A., Grevendonk, W., and Herreman, W. (1967). *Physica (Utrecht)* **37**, 227.

Erginsoy, C., Vineyard, G. H., and Englert, A. (1964). *Phys. Rev.* **133**, A595.

Fermi, E., Pasta, J. G., and Ulam, S. M. (1955). "Studies of Nonlinear Problems," LASL Report LA-1940; also available in "Enrico Fermi. Collected Papers," Vol. II, p. 978. Univ. of Chicago Press, Chicago, Illinois, 1965.

Ford, J. (1973). *Advan. Chem. Phys.* **24**, 155.

Gass, D. (1969). *J. Chem. Phys.* **51**, 4560.

Gehlen, P. C., Beeler, J. R., and Jaffee, R. I., eds. (1972). "Interatomic Potentials and Simulation of Lattice Defects." Plenum, New York.

Gibbons, T. G., and Klein, M. L. (1974). *J. Chem. Phys.* **60**, 112.

Gibson, J. B., Goland, A. N., Milgram, M., and Vineyard, G. H. (1960). *Phys. Rev.* **120**, 1229.

Gosling, E. M., McDonald, I. R., and Singer, K. (1973). *Mol. Phys.* **26**, 1475.

Green, M. S. (1952). *J. Chem. Phys.* **20**, 1281.

Guichelaar, J., van Leeuwen, W. A., and de Groot, S. R. (1973). *Physica (Utrecht)* **68**, 342.

Hanley, H. J. M., McCarty, R. D., and Cohen, E. G. D. (1972). *Physica (Utrecht)* **60**, 322.

Hansen, J. P., and Verlet, L. (1969). *Phys. Rev.* **184**, 151.

Hansen, J. P., and Weis, J. J. (1969). *Phys. Rev.* **188**, 314.

Harp, G. D., and Berne, B. J. (1968). *J. Chem. Phys.* **49**, 1249.

Haynes, W. M. (1973). *Physica (Utrecht)* **67**, 440.

Helfand, E. (1960). *Phys. Rev.* **119**, 1.

Hellemans, J., Zink, H., and Van Paemel, O. (1970). *Physica (Utrecht)* **46**, 395.

Henderson, D., and Barker, J. A. (1970). *Phys. Rev. A* **1**, 1266.

Hirschfelder, J. O., Curtiss, C. F., and Bird, R. B. (1954). "Molecular Theory of Gases and Liquids." Wiley, New York.

Hohl, F. (1972). *In* "Gravitational *N*-Body Problem" (M. Lecar, ed.), p. 431. Reidel, Dordrecht, Netherlands.

Hoover, W. G., and Alder, B. J. (1967). *J. Chem. Phys.* **46**, 686.

Hoover, W. G., Ross, M., Johnson, K. W., Henderson, D., Barker, J. A., and Brown, B. C. (1970). *J. Chem. Phys.* **52**, 4931.

Hoover, W. G., Ashurst, W. T., and Olness, R. J. (1974). *J. Chem. Phys.* **60**, 4043.

Keyes, T., and Oppenheim, I. (1973). *Phys. Rev. A* **8**, 937.

Kubo, R. (1957). *J. Phys. Soc. Jap.* **12**, 570.

Lecar, M. (1972). *In* "Gravitational N-Body Problem" (M. Lecar, ed.), p. 42. Reidel Publ., Dordrecht, Netherlands.

Lee, J. K., Barker, J. A., and Pound, G. M. (1974). *J. Chem. Phys.* **60**, 1976.

Lees, A. W., and Edwards, S. F. (1972). *J. Phys. C* **5**, 1921.

Levesque, D., and Ashurst, W. T. (1974). *Phys. Rev. Lett.* **33**, 277.

Levesque, D., Verlet, L., and Kurkijarvi, J. (1973). *Phys. Rev. A* **7**, 1690.

McLaughlin, E., and Horrocks, J. K. (1964). *Chem. Rev.* **64**, 389.

Mansoori, G. A., and Canfield, F. B. (1969). *J. Chem. Phys.* **51**, 4958.

Mayer, J. E., and Mayer, M. G. (1940). "Statistical Mechanics." Wiley, New York.

Michels, A., Schipper, A. C. J., and Rintoul, W. H. (1953). *Physica (Utrecht)* **19**, 1011.

Partington, J. R. (1955). "An Advanced Treatise on Physical Chemistry. II. The Properties of Liquids." Longmans, Green, New York.

Paskin, A., and Dienes, G. J. (1972). *J. Appl. Phys.* **43**, 1605.

Rahman, A. (1964). *Phys. Rev.* **136**, A405.

Rahman, A., Fowler, R. H., and Narten, A. H. (1972). *J. Chem. Phys.* **57**, 3010.

Rasaiah, J., and Stell, G. (1970). *Mol. Phys.* **18**, 249.

Ree, F. H. (1971). *In* "Physical Chemistry" (D. Henderson, ed.), Vol. 8A, Chapter 3, p. 157. Academic Press, New York.

Ree, F. H., Ree, T., and Eyring, H. (1958). *Ind. Eng. Chem.* **50**, 1036.

Schlichting, H. (1960). "Boundary Layer Theory," p. 491. McGraw-Hill. New York.

Sisko, A. W. (1958). *Ind. Eng. Chem.* **50**, 1789.

Tsai, D. H., and Beckett, C. W. (1966). *J. Geophys. Res.* **71**, 2601.

Tuck, J. L., and Menzel, M. T. (1972). *Advan. Math.* **9**, 399.

Verlet, L. (1967). *Phys. Rev.* **159**, 98.

Vineyard, G. H. (1972). *In* "Interatomic Potentials and Simulation of Lattice Defects" (P. C. Gehlen, J. R. Beeler, and R. I. Jaffee, eds.), p. 3. Plenum, New York.

Visscher, W. M. (1973). *Phys. Rev. A* **7**, 1439.

Wainwright, T. E., and Alder, B. J. (1958). *Nuovo Cimento, Suppl.* **9**, 116.

Wood, W. W. (1968). *In* "The Physics of Simple Liquids" (H. N. V. Temperley, J. R. Rowlinson, and G. S. Rushbrooke, eds.), Chapter 5, p. 115. North-Holland Publ., Amsterdam.

Wood, W. W. (1973). *Acta Phys. Austr., Suppl.* **10**, 451.

Wood, W. W., Parker, F. R., and Jacobson, J. D. (1958). *Nuovo Cimento, Suppl.* **9**, 133.

Zwanzig, R. (1965). *Annu. Rev. Phys. Chem.* **16**, 67.